INTERACTION NOTES

Note 187

May 1968

GENERALIZED NETWORK PARAMETERS FOR BODIES OF REVOLUTION

by

Joseph R. Mautz
Roger F. Harrington

Syracuse University
Syracuse, New York

ABSTRACT

The problem of electromagnetic radiation and scattering from perfectly conducting bodies of revolution of arbitrary shape is considered. The mathematical formulation is an integro-differential equation, obtained from the potential integrals plus boundary conditions at the body. A solution is effected by the method of moments, and the results are expressed in terms of generalized network parameters. A computer program for computing the generalized impedance matrix of an arbitrary body of revolution is included.

The expansion functions chosen for the moment solutions are harmonic in ϕ (azimuth angle) and subsectional in t (contour length variable). Because of rotational symmetry, the solution becomes a Fourier series in ϕ, each term of which is uncoupled to every other term. Hence, the problem reduces to a set of independent modes, one for each harmonic term.

Illustrative computations are given for radiation from apertures and plane-wave scattering from bodies of revolution. The impedance elements, currents, radiation patterns, and scattering patterns for a conducting sphere are computed both from the general program and from the classical eigenfunction

ABSTRACT (Con't)

solution. The agreement obtained serves to check the general program. Similar computations for a cone-sphere illustrate the application of the general program to problems not solvable by classical methods.

CONTENTS

I. INTRODUCTION

Determination of the behavior of a conducting body in a known impressed field is a fundamental problem of applied electromagnetic theory. Specific examples are scattering by conducting objects and radiation from conducting antennas. A general procedure for treating such problems is given by the method of moments.[1,2] This is a procedure for reducing the functional problem to a finite dimensional matrix problem. In electromagnetic theory, the resultant matrices can be identified as generalized network parameters.[3] Once the generalized impedance matrix of a body is known, the behavior of that body for arbitrary excitation is easily calculated by matrix manipulations. Furthermore, the effect of impedance loading can be accounted for by constraints on the matrix equations.[2,4,5]

The problem is formulated in the conventional way as follows. Let $\underline{E}^i$ denote the known impressed field and $\underline{E}^s$ the scattered field due to currents on the body. Then the total field $\underline{E}$ is the sum of the impressed and scattered fields, that is,

$$\underline{E} = \underline{E}^i + \underline{E}^s \tag{1}$$

The scattered field can be expressed in terms of a vector potential $\underline{A}$ and scalar potential Φ as

$$\underline{E}^s = -j\omega\underline{A} - \nabla\Phi \tag{2}$$

where

$$\underline{A} = \mu \iint_S \underline{J} \frac{e^{-jkR}}{4\pi R} \, ds \tag{3}$$

$$\Phi = \frac{1}{\epsilon} \iint_S \sigma \frac{e^{-jkR}}{4\pi R} \, ds \tag{4}$$

Here S is the surface of the conductor, R is the distance from a source point to the field point, $\underset{\sim}{J}$ is the surface current on S, and σ is the surface charge on S. The current and charge are related by the equation of continuity

$$\nabla \cdot \underset{\sim}{J} = -j\omega\sigma \tag{5}$$

The boundary condition requires that the tangential component of total $\underset{\sim}{E}$ vanish on S. Hence,

$$\underset{\sim}{E}^{i}_{tan} = -\underset{\sim}{E}^{s}_{tan} \tag{6}$$

where the subscript tan denotes tangential component on S. The problem can now be stated succinctly as

$$L(\underset{\sim}{J}) = \underset{\sim}{E}^{i}_{tan} \tag{7}$$

where L is the integro-differential operator

$$L(\underset{\sim}{J}) = [j\omega\underset{\sim}{A} + \nabla\Phi]_{tan} \tag{8}$$

A solution of (7) gives the current $\underset{\sim}{J}$ on S. Usually we are interested in some functional of $\underset{\sim}{J}$, which can be computed once $\underset{\sim}{J}$ is known.

This report considers the special case of bodies which are rotationally symmetric about an axis. Because of this symmetry a Fourier series expansion in the angle of rotational symmetry reduces the problem to a system of independent modes. This is important from the standpoint of computation, because it is faster to invert several small matrices instead of one large one. The particular case of scattering by conducting bodies of revolution has been treated previously by Andreasen.[6] His solution is conceptually similar to ours, but differs in detail.

II. METHOD OF SOLUTION

To effect a solution of (7) we use the method of moments, which is closely related to Galerkin's method.[1,2] This procedure approximates (7) by a matrix equation, which can then be inverted by known algorithms. The matrix so obtained is a generalized impedance matrix for the body.[3] The excitation of the body is represented by a voltage matrix, and the resultant current on the body is represented by a current matrix.

For the method of moments, let the inner product be defined as

$$\langle \underline{W}, \underline{J} \rangle = \oiint_S \underline{W} \cdot \underline{J} \, ds \tag{9}$$

where $\underline{W}$ and $\underline{J}$ are tangential vectors on S. A set of expansion functions $\{\underline{J}_j\}$ is next defined, and the current on S approximated by

$$\underline{J} = \sum_j I_j \underline{J}_j \tag{10}$$

where I_j are constants to be determined. Equation (10) is substituted into (7), which, because of the linearity of L, reduces to

$$\sum_j I_j L\underline{J}_j = \underline{E}^i_{tan} \tag{11}$$

A set of testing functions $\{\underline{W}_i\}$ is defined, and the inner product of (11) with each $\underline{W}_i$ is taken. The result is

$$\sum_j I_j \langle \underline{W}_i, L\underline{J}_j \rangle = \langle \underline{W}_i, \underline{E}^i \rangle \tag{12}$$

$i = 1,2,3,\ldots$. The subscript tan has been dropped from $\underset{\sim}{E}^i$ because the inner product involves only tangential components. We now define the generalized network matrices

$$[Z] = [< \underset{\sim}{W}_i, L\underset{\sim}{J}_j >] \tag{13}$$

$$[V] = [< \underset{\sim}{W}_i, \underset{\sim}{E}^i >] \tag{14}$$

$$[I] = [I_i] \tag{15}$$

and rewrite the set (12) as

$$[Z]\,[I] = [V] \tag{16}$$

$[Z]$ is the generalized impedance matrix, and $[Y] = [Z]^{-1}$ is the generalized admittance matrix. The inverse of (16)

$$[I] = [Y]\,[V] \tag{17}$$

gives the coefficients I_j of the current expansion (10), and hence is an approximate solution to the problem.

The impedance elements of (13) are explicitly

$$Z_{ij} = \iint_S \underset{\sim}{W}_i \cdot (j\omega\underset{\sim}{A}_j + \nabla\Phi_j)\, ds \tag{18}$$

where we have used (8) and (9). The subscript j denotes that $\underset{\sim}{A}_j$ and Φ_j are the potentials due to $\underset{\sim}{J}_j$ and σ_j. If the two-dimensional divergence theorem is applied to the vector $\Phi\underset{\sim}{W}_i$ on a closed surface, the following identity results:

$$\iint_S \nabla\Phi \cdot \underset{\sim}{W}_i\, ds = -\iint_S \Phi\nabla \cdot \underset{\sim}{W}_i\, ds \tag{19}$$

If $\underline{W}$ is thought of as a current, the charge associated with it is

$$\sigma_i = \frac{-1}{j\omega} \underline{\nabla} \cdot \underline{W}_i \tag{20}$$

Now (18) can be written as

$$Z_{ij} = j\omega \oiint_S (\underline{W}_i \cdot \underline{A}_j + \sigma_i \Phi_j) \, ds \tag{21}$$

Equation (21) is more convenient for computation than (18) because the gradient operation on Φ has been eliminated.

So far the discussion has been for an arbitrary conducting body. Henceforth we restrict consideration to surfaces S generated by revolving a plane curve about the z axis. The surface and coordinate system are shown in Figure 1. Here ρ, ϕ, z are the usual cylindrical coordinate variables, and t is a length variable along the curve generating S. We desire the expansion (10) to be general enough to approximate an arbitrary $\underline{J}$ on S. Hence, independent sets of functions are defined as

$$\begin{aligned} \underline{J}^t_{mj} &= \underline{u}_t \, f_j(t) \, e^{jm\phi} \\ \underline{J}^\phi_{mj} &= \underline{u}_\phi \, f_j(t) \, e^{jm\phi} \end{aligned} \tag{22}$$

where $\underline{u}_t$ and $\underline{u}_\phi$ are unit vectors t-directed and ϕ-directed, respectively. We have chosen the f_j in both sets to be the same, but it is not necessary to do so. The current expansion (10) now becomes

$$\underline{J} = \sum_{m,j} (I^t_{mj} \, \underline{J}^t_{mj} + I^\phi_{mj} \, \underline{J}^\phi_{mj}) \tag{23}$$

For testing functions, choose

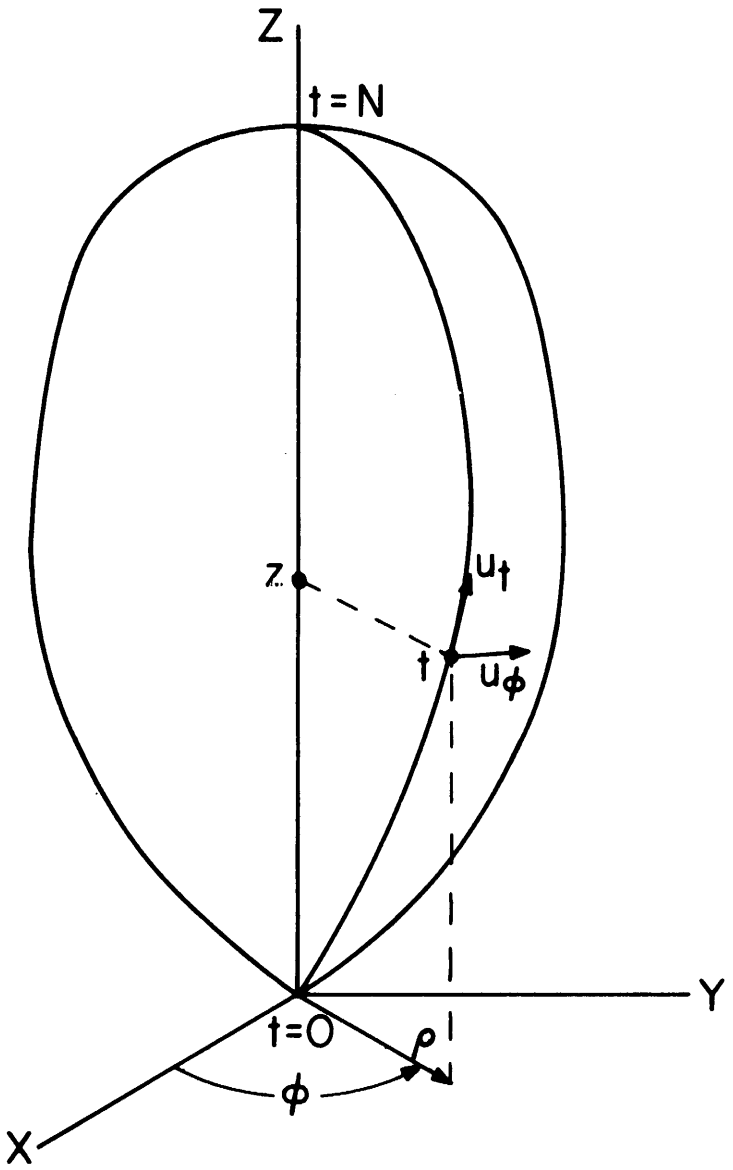

Figure 1. Body of revolution and coordinate system.

$$\underset{\sim}{W}^{t}_{ni} = \underset{\sim}{u}_{t}\, f_i(t)\, e^{-jn\phi}$$

$$\underset{\sim}{W}^{\phi}_{ni} = \underset{\sim}{u}_{\phi}\, f_i(t)\, e^{-jn\phi} \qquad (24)$$

which differ from (22) only in the sign of the exponent. The $\underset{\sim}{W}_n$ are orthogonal to $\underset{\sim}{J}_m$, $m \neq n$, over 0 to 2π on ϕ, and also to $L\underset{\sim}{J}_m$ (the field from $\underset{\sim}{J}_m$). Hence, all impedance elements are zero except those for which m = n, and each mode can be treated separately. This is the major simplification introduced by the rotational symmetry of the body.

The use of (22) and (24) to evaluate the elements of (21) results in the partitioned matrix equation

$$\begin{bmatrix} [Z_n^{tt}] & [Z_n^{t\phi}] \\ [Z_n^{\phi t}] & [Z_n^{\phi\phi}] \end{bmatrix} \begin{bmatrix} [I_n^{t}] \\ [I_n^{\phi}] \end{bmatrix} = \begin{bmatrix} [V_n^{t}] \\ [V_n^{\phi}] \end{bmatrix} \qquad (25)$$

Here the elements of the Z submatrices are

$$(Z_n^{tt})_{ij} = \langle \underset{\sim}{W}^{t}_{ni},\ L\underset{\sim}{J}^{t}_{nj} \rangle$$

$$(Z_n^{t\phi})_{ij} = \langle \underset{\sim}{W}^{t}_{ni},\ L\underset{\sim}{J}^{\phi}_{nj} \rangle$$

$$(Z_n^{\phi t})_{ij} = \langle \underset{\sim}{W}^{\phi}_{ni},\ L\underset{\sim}{J}^{t}_{nj} \rangle \qquad (26)$$

$$(Z_n^{\phi\phi})_{ij} = \langle \underset{\sim}{W}^{\phi}_{ni},\ L\underset{\sim}{J}^{\phi}_{nj} \rangle$$

the elements of the V submatrices are

$$(V_n^t)_i = \langle W_{ni}^t, \underline{E}^i \rangle$$
$$(V_n^\phi)_i = \langle W_{ni}^\phi, \underline{E}^i \rangle \qquad (27)$$

and the elements of the I submatrices are the coefficients in (23). Note that, for N terms in the Fourier series on ϕ, there are N sets of matrix equations (25).

The solution to (25) can also be written in partitioned form as

$$\begin{bmatrix} [V_n^t] \\ [V_n^\phi] \end{bmatrix} = \begin{bmatrix} [Y_n^{tt}] & [Y_n^{t\phi}] \\ [Y_n^{\phi t}] & [Y_n^{\phi\phi}] \end{bmatrix} \begin{bmatrix} [I_n^t] \\ [I_n^\phi] \end{bmatrix} \qquad (28)$$

The Y submatrices must in general be obtained after inversion of the entire Z matrix, and are not the inverses of corresponding Z submatrices. However, the -n mode matrices are related to the +n mode matrices by

$$\begin{bmatrix} [Y_{-n}^{tt}] & [Y_{-n}^{t\phi}] \\ [Y_{-n}^{\phi t}] & [Y_{-n}^{\phi\phi}] \end{bmatrix} = \begin{bmatrix} [Y_n^{tt}] & [-Y_n^{t\phi}] \\ [-Y_n^{\phi t}] & [Y_n^{\phi\phi}] \end{bmatrix} \qquad (29)$$

Hence, only the $n \geq 0$ mode matrices need be inverted. The proof of (29) follows from the fact that the Z matrices satisfy the same equation (see next section), and this symmetry survives matrix inversion.

Finally, for an explicit solution we must choose the $f_i(t)$, the t expansion functions. It is known that subsectional expansions, using pulse functions or triangle functions, give well-conditioned matrices.[2] The current must be

differentiated to obtain the charge; hence it is preferable to use triangle functions. Furthermore, a triangle expansion gives a piecewise-linear approximation which converges about twice as fast as a step approximation.[1,2] Finally, if $\rho\underline{J}$ is expanded in triangles instead of $\underline{J}$, the divergence formula and the treatment of the end points of t become simpler. Hence, we chose

$$f_i(t) = \frac{1}{\rho} T(t-t_i) \tag{30}$$

where T is the triangle function

$$T(t) = \begin{cases} 1 - |t|, & |t| < 1 \\ 0 & |t| > 1 \end{cases} \tag{31}$$

When using these functions, distance and frequency are scaled so that the t_i are one unit apart. As in Figure 1, t is zero at the lower pole and N at the upper pole. There are (N-1) triangle functions with peaks at 1,2,3...N-1.

Numerical evaluation of the impedance elements is quite difficult because of the complexity of the formulas. An approximate evaluation was obtained by approximating each triangle function by four steps. The potential integrals due to each step are evaluated at the center of all steps by a numerical integration. The second integration, represented by (18), is then approximated by the value of the integrand at the center of each step, summed over the four step approximation to the testing triangle. The details of the solution are given in the next section, and the computer program and instructions for using it are given in Appendix A.

III. EVALUATION OF THE IMPEDANCES

The generalized impedances for a body are given by (21), which can be written in greater detail as

$$Z_{ij} = \oiint_S ds' \oiint_S ds \left[j\omega\mu \, \underset{\sim}{W}_i \cdot \underset{\sim}{J}_j + \frac{1}{j\omega\epsilon} (\underset{\sim}{\nabla}' \cdot \underset{\sim}{W}_i)(\underset{\sim}{\nabla} \cdot \underset{\sim}{J}_j) \right] \frac{e^{-jkR}}{4\pi R} \tag{32}$$

This is valid for bodies of arbitrary shape. For bodies of revolution,

$$\oiint_S ds = \int_0^N dt \int_0^{2\pi} d\phi \; \rho(t) \tag{33}$$

$$\underset{\sim}{\nabla} \cdot \underset{\sim}{J} = \frac{1}{\rho} \frac{\partial}{\partial t} (\rho J_t) + \frac{1}{\rho} \frac{\partial}{\partial \phi} (J_\phi) \tag{34}$$

$$R = \sqrt{\rho^2 + \rho'^2 - 2\rho\rho' \cos(\phi - \phi') + (z - z')^2} \tag{35}$$

Four types of impedances are defined by (26). To evaluate them, we use (22) and (24) to obtain the $\underset{\sim}{W} \cdot \underset{\sim}{J}$ terms in (32) as

$$\underset{\sim}{W}^p_{ni} \cdot \underset{\sim}{J}^q_{nj} = e^{jn(\phi-\phi')} \, f_i(t') \, f_j(t) \, \underset{\sim}{u}'_p \cdot \underset{\sim}{u}_q \tag{36}$$

where p and q represent permutations of t and ϕ. The unit vector dot products, in terms of the body coordinates defined by Figure 1, are

$$
\begin{aligned}
\underline{u}_t' \cdot \underline{u}_t &= \sin v \sin v' \cos(\phi-\phi') + \cos v \cos v' \\
\underline{u}_t' \cdot \underline{u}_\phi &= -\sin v' \sin(\phi-\phi') \\
\underline{u}_\phi' \cdot \underline{u}_t &= \sin v \sin (\phi-\phi') \\
\underline{u}_\phi' \cdot \underline{u}_\phi &= \cos(\phi-\phi')
\end{aligned}
\tag{37}
$$

Here v is the angle between the t direction and the z axis, being positive if $\underline{u}_t$ points away from the z axis and negative if $\underline{u}_t$ points toward it. Changing $(\phi-\phi')$ to a new variable, and expressing the sine and cosine terms of (37) as exponentials, one ϕ integration in (32) can be performed. The remaining ϕ integration defines the Green's function.[6]

$$
g_n = \int_0^\pi d\phi \, \frac{e^{-jkR_o}}{R_o} \cos n\phi \tag{38}
$$

where R_o is given by (35) with $\phi' = 0$. With f_i given by (30), the resultant expressions for the impedance elements (26) are

$$(Z_n^{tt})_{ij} = \int_0^N dt' \int_0^N dt \left[j\omega\mu T(t'-i)\, T(t-j)(\sin v \sin v' \frac{g_{n+1} + g_{n-1}}{2} + \cos v \cos v'\, g_n) + \frac{1}{j\omega\epsilon} T'(t'-i)\, T'(t-j) g_n \right]$$

$$(Z_n^{t\phi})_{ij} = \int_0^N dt' \int_0^N dt \left[-\omega\mu T(t'-i)\, T(t-j) \sin v' \frac{g_{n+1} - g_{n-1}}{2} + \frac{n}{\omega\epsilon\rho} T'(t'-i)\, T(t-j)\, g_n \right]$$

$$(Z_n^{\phi t})_{ij} = \int_0^N dt' \int_0^N dt \left[+\omega\mu T(t'-i)\, T(t-j) \sin v \frac{g_{n+1} - g_{n-1}}{2} - \frac{n}{\omega\epsilon\rho'} T(t'-i)\, T'(t-j)\, g_n \right] \qquad (39)$$

$$(Z_n^{\phi\phi})_{ij} = \int_0^N dt' \int_0^N dt \left[j\omega\mu T(t'-i)\, T(t-j) \frac{g_{n+1} + g_{n-1}}{2} + \frac{n^2}{j\omega\epsilon\rho\rho'} T(t'-i)\, T(t-j)\, g_n \right]$$

Here T' is the derivative of a triangle function

$$T'(t) = \begin{cases} 1, & -1 < t < 0 \\ -1, & 0 < t < 1 \\ 0, & |t| > 1 \end{cases} \qquad (40)$$

which is a pulse doublet. Further evaluation of (39) is done by numerical methods.

The integrations of (39) involve many different integrands, and to reduce the number of integrations the following approximations are made. For

the t integration, the T function is approximated by four pulses of amplitudes 1/4, 3/4, 3/4, 1/4, as shown in Figure 2(a). The derivative of T is represented exactly by four pulses of amplitude 1, 1, -1, -1, as shown in Figure 2(b). The functions ρ, sin v, and cos v are assumed constant over each pulse, equal to their values at the midpoint of the pulse. For the t' integration, the T function is approximated by four impulse functions, of strengths 1/8, 3/8, 3/8, 1/8, as shown in Figure 2(a). The derivative of T is approximated by four impulse functions of strengths 1/2, 1/2, -1/2, -1/2, as shown in Figure 2(b). We now define the numbers

$$\begin{aligned} T_1 &= 1/8 & T_1' &= 1/2 \\ T_2 &= 3/8 & T_2' &= 1/2 \\ T_3 &= 3/8 & T_3' &= -1/2 \\ T_4 &= 1/8 & T_4' &= -1/2 \end{aligned} \tag{41}$$

the midpoints of the pulses

$$t_p = i + \frac{p - 2.5}{2} \qquad t_q = j + \frac{q - 2.5}{2} \tag{42}$$

and the pulse Green's functions

$$G_n = 2 \int_{j + \frac{q-3}{2}}^{j + \frac{q-2}{2}} dt \int_0^{\pi} d\phi \, \frac{e^{-jkR_p}}{R_p} \cos n\phi \tag{43}$$

$$R_p = \sqrt{\rho^2 + \rho_p^2 - 2\rho\rho_p \cos \phi + (z - z_p)^2} \tag{44}$$

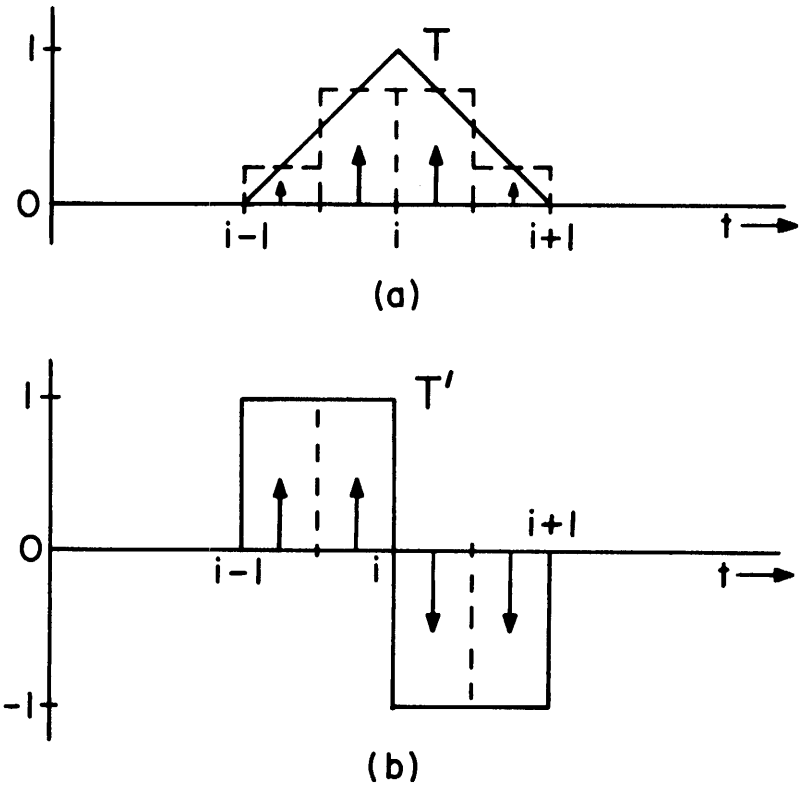

Figure 2. (a) Triangle function (solid), four-pulse approximation (dashed), impulse approximation (arrows). (b) Derivative of triangle function (solid), four-pulse representation (dashed), impulse approximation (arrows).

In terms of these definitions and approximations, the matrix elements (39) reduce to

$$(Z_n^{tt})_{ij} = \sum_{p=1}^{4}\sum_{q=1}^{4}\left[j\omega\mu\, T_pT_q\left(\sin v_p \sin v_q \frac{G_{n+1}+G_{n-1}}{2} + \cos v_p \cos v_q\, G_n\right) + \frac{1}{j\omega\epsilon}\, T'_pT'_q\, G_n\right]$$

$$(Z_n^{t\phi})_{ij} = \sum_{p=1}^{4}\sum_{q=1}^{4}\left[-\omega\mu\, T_pT_q \sin v_p \frac{G_{n+1}-G_{n-1}}{2} + \frac{n}{\omega\epsilon}\, T'_p \frac{T_q}{\rho_q}\, G_n\right] \qquad (45)$$

$$(Z_n^{\phi t})_{ij} = \sum_{p=1}^{4}\sum_{q=1}^{4}\left[+\omega\mu\, T_pT_q \sin v_q \frac{G_{n+1}-G_{n-1}}{2} - \frac{n}{\omega\epsilon}\frac{T_p}{\rho_p}\, T'_q\, G_n\right]$$

$$(Z_n^{\phi\phi})_{ij} = \sum_{p=1}^{4}\sum_{q=1}^{4}\left[j\omega\mu\, T_pT_q \frac{G_{n+1}+G_{n-1}}{2} + \frac{n^2}{j\omega\epsilon}\frac{T_p}{\rho_p}\frac{T_q}{\rho_q}\, G_n\right]$$

Here ρ_p, v_p, ρ_q, v_q are the ρ and v evaluated at t_p and t_q respectively.

Finally, we evaluate the G_n of (43) by a combination of analytical and numerical techniques as follows. The interval $0 < \phi < \pi$ is divided into M equal intervals, and (43) approximated by

$$G_n = \frac{2\pi}{M}\sum_{m=1}^{M} \cos n\phi_m \int_{j+\frac{q-3}{2}}^{j+\frac{q-2}{2}} dt\, \frac{e^{-jkR_p}}{R_p} \qquad (46)$$

where $\phi_m = (m - \frac{1}{2})\,\pi/M$. The R_p of (46) is evaluated at $\phi = \phi_m$. Define

$$R_{pq} = \sqrt{\rho_p^2 + \rho_q^2 - 2\rho_p\rho_q \cos\phi_m + (z_p - z_q)^2} \qquad (47)$$

Then $|R_p - R_{pq}| \leq 1/4$. If the distance between peaks of the triangle functions is a tenth of a wavelength, then $k|R_p - R_{pq}| \leq \pi/20$, and $\exp(-jkR_p)$ may be represented by two terms of its Taylor expansion about R_{pq}. This gives

$$G_n = \frac{2\pi}{M} \sum_{m=1}^{M} \cos n\phi_m \, e^{-jkR_{pq}} \int_{j+\frac{q-3}{2}}^{j+\frac{q-2}{2}} dt \, \frac{1 - jk(R_p - R_{pq})}{R_p} \tag{48}$$

For the final integration, we approximate t by a straight line between $t = j + \frac{q-3}{2}$ and $t = j + \frac{q-2}{2}$. Then z and ρ are linear in t, and the integrand of (48) can be simplified by completing the square. This gives

$$G_n = \frac{2\pi}{M} \sum_{m=1}^{M} \cos n\phi_m \, e^{-jkR_{pq}} \int_{t_o - 1/4}^{t_o + 1/4} dt \, \frac{1 - jk(\sqrt{t^2+d^2} - R_{pq})}{\sqrt{t^2 + d^2}} \tag{49}$$

where

$$t_o = |(z_p - z_q) \cos v_q + (\rho_p \cos \phi_m - \rho_q) \sin v_q| \tag{50}$$

$$d^2 = R_{pq}^2 - t_o^2 \tag{51}$$

The integration of (49) is now straightforward, and one obtains[7]

$$G_n = \frac{\pi}{M} \sum_{m=1}^{M} \cos n\phi_m \, f(\phi_m) \tag{52}$$

where

$$f(\phi_m) = e^{-jkR_{pq}} \left[2(1+jkR_{pq}) \log \frac{t_2 + \sqrt{t_2^2+d^2}}{t_1 + \sqrt{t_1^2+d^2}} - jk \right] \tag{53}$$

and

$$t_1 = t_o - \frac{1}{4} \qquad t_2 = t_o + \frac{1}{4} \tag{54}$$

This completes the evaluation of the impedances.

Some computational details will now be discussed. In (54), if t_o is larger than 1/4 both t_1 and t_2 are positive, but if t_o is less than 1/4, t_1 is negative. In this case the log term of (53) should be replaced by

$$\log \frac{(t_2 + \sqrt{t_2^2 + d^2})\ (-t_1 + \sqrt{t_1^2 + d^2})}{d^2} \tag{55}$$

G_n is the scalar potential due to a charge distribution on the lateral surface of a frustum. The approximation (46) supposes line charges at ϕ_m. If the source point is very close to the field point, the granular nature of the line charges may be too restrictive. When the source and field points coincide on the first interval $0 \le \phi \le \frac{\pi}{M}$, the line charge at $\phi = \frac{\pi}{2M}$ is spread out into a uniform surface charge. Furthermore, if the surface of this first interval is approximated by a plane rectangle of dimension 1/2 by $\frac{\rho_q \pi}{M}$,

$$G_n = \frac{4}{\rho_q} \int_0^{1/4} dy \int_0^{\frac{\rho_q \pi}{M}} dx \frac{1-jk\sqrt{x^2+y^2}}{\sqrt{x^2+y^2}} + \sum_{m=2}^{M} \cos n\phi_m\ f(\phi_m). \tag{56}$$

Now, since

$$\frac{\partial^2}{\partial x \partial y} \left[x \log(y + \sqrt{y^2 + x^2}) + y \log(x + \sqrt{y^2 + x^2}) \right] = \frac{1}{\sqrt{x^2+y^2}}\ , \tag{57}$$

one can reduce (56) to

$$G_n = -\frac{4}{\rho_q}\left[x_o \log\left(\frac{y_o+\sqrt{y_o^2+x_o^2}}{x_o}\right) + y_o \log\left(\frac{x_o+\sqrt{y_o^2+x_o^2}}{y_o}\right)\right]\frac{-jkx_o}{\rho_q} + \sum_{m=2}^{M} \cos n\phi_m \, f(\phi_m) \tag{58}$$

where

$$x_o = \frac{\rho_q \pi}{M}, \qquad y_o = 1/4 \tag{59}$$

A more elaborate method involving a localized increase in the density of line charges was attempted but was abandoned when the results did not differ appreciably from (58).

IV. COMPUTATION OF IMPEDANCES

Equation (45) for the impedances has been programmed in Fortran IV for execution on an IBM System/360 Model 50 computer. Appendix A lists the computer program and all its printed output for the first mode (n=1 in (45)) for a sphere of radius $\frac{10}{\pi}$ and radius to wavelength ratio 0.2. Also included in Appendix A are instructions for the use of the computer program along with some explanatory notes to facilitate possible modifications. In the interest of simplicity, the program is written to compute one mode at a time. Input data consists of the mode number, the total length (an integer determining the size of the impedance matrix desired) of the curve that generates the surface S, an integer telling how many times to subdivide the ϕ axis between 0° and 180° for the G_n of (52), the wave constant $\frac{2\pi}{\lambda}$, and some arrays defining the angle between the tangent to the generating curve and the z axis, the cylindrical coordinate radius ρ of the generating curve and z the axial distance from the start of the generating curve at the lower pole. The output consists of some of the G_n of (52), the impedance matrix Z, and its inverse the admittance matrix Y, as explained in Appendix A.

To check the accuracy of the program, the impedance for current on a sphere has been evaluated by spherical mode expansions. The details of the solution are given in Mautz's thesis.[13] The final result for any mode with $e^{jm\phi}$ variation on a sphere of radius a is

$$(Z_m^{tt})_{ij} = \sum_{n=|m|}^{\infty} \frac{1}{D_{mm}} \left[\lambda_n^{TE} b_{ni} b_{nj} + \lambda_n^{TM} c_{ni} c_{nj} \right]$$

$$(Z_m^{\phi t})_{ij} = j \sum_{n=|m|}^{\infty} \frac{1}{D_{mn}} \left[\lambda_n^{TE} c_{ni} b_{nj} + \lambda_n^{TM} b_{ni} c_{nj} \right] \qquad (60)$$

$$(Z_m^{t\phi})_{ij} = -(Z_m^{\phi t})_{ji}$$

$$(Z_m^{\phi\phi})_{ij} = \sum_{n=|m|}^{\infty} \frac{1}{D_{mn}} \left[\lambda_n^{TE} c_{ni} c_{nj} + \lambda_n^{TM} b_{ni} b_{nj}\right]$$

where

$$D_{mn} = \frac{4\pi a^2 (n)(n+1)(n+m)!}{(2n+1)(n-m)!} \tag{61}$$

The eigenvalues are given in terms of alternate spherical Bessel functions as

$$\begin{aligned} \lambda_n^{TE} &= \eta \hat{J}_n(ka) \hat{H}_n^{(2)}(ka) \\ \lambda_n^{TM} &= \eta \hat{J}_n'(ka) \hat{H}_n^{(2)'}(ka) \end{aligned} \tag{62}$$

The b and c coefficients are

$$\begin{aligned} b_{nj} &= -2\pi a^2 m \int_0^{\pi} P_n^m(\cos\theta) f_j(t) \, d\theta \\ c_{nj} &= 2\pi a^2 \int_0^{\pi} \frac{\partial P_n^m(\cos\theta)}{\partial\theta} \sin\theta \, f_j(t) \, d\theta \end{aligned} \tag{63}$$

where $f_j(t)$ is the j^{th} expansion function as defined in general by (22) and in particular by (30). The P_n^m in (63) are the associated Legendre polynomials. The evaluation of (63) was done numerically.

Table 1

Comparison of impedance elements on a sphere of radius 0.2λ, using 9 expansion triangles, n = 1 mode.

Impedance element	Formula (45) of Section III	18 TE and TM modes in (60)	9 TE and TM modes in (60)
Z_{11}^{tt}	53.46 - j2477.	53.36 - j1908	53.36 - j616.5
Z_{55}^{tt}	26.80 - j768.9	26.83 - j701.0	26.83 - j567.9
Z_{15}^{tt}	10.26 + j52.28	10.08 + j52.36	10.08 + j151.8
$Z_{11}^{\phi\phi}$	57.67 - j2641	57.36 - j2236.	57.36 - j1754
$Z_{55}^{\phi\phi}$	32.90 + j9.467	32.93 + j11.05	32.93 + j9.903
$Z_{15}^{\phi\phi}$	29.26 - j34.36	29.27 - j34.32	29.27 - j40.57
$Z_{11}^{t\phi}$	1569. - j54.88	1100. - j55.08	321.6 - j55.08
$Z_{55}^{t\phi}$	$(-1.68 + j.343)\times10^{-4}$	$(-2.12 + j.405)\times10^{-5}$	$(-2.48 + j.405)\times10^{-5}$
$Z_{15}^{t\phi}$	-37.15 - j27.17	-37.13 - j27.25	-27.87 - j27.25

Table 1 shows representative computations for a sphere of radius $a = 0.2\lambda$, using 9 equispaced triangles. In other words, the expansion functions are (30) with the $t_i = 1,2,\ldots,9$, and the z axis cuts the sphere at $t_i = 0$ and 10. The M appearing in (52) is twenty. The mode chosen is n = 1 in (45), and correspondingly, m = 1 in (60). Column 1 of Table 1 gives the computation using the general solution (45) of Section III. Column 2 gives the solution using 18 terms of the infinite series (60). Column 3 uses 9 terms of the series (60). Notice that the real parts of Z^{tt} and $Z^{\phi\phi}$ and the imaginary part of $Z^{t\phi}$ are identical for the 18 term and 9 term solution of (60) and are only slightly different from those of (45). The imaginary parts of Z^{tt} and $Z^{\phi\phi}$ and the real parts of $Z^{\phi t}$ and $Z^{t\phi}$ of (60) are converging very slowly in the modal solution, but are converging towards the corresponding parts of the general solution. $Z_{55}^{t\phi}$ is supposed to be zero, and the non zero values of $Z_{55}^{t\phi}$ in Table 1 are so small that all the significant figures are probably meaningless. On the basis of comparisons such as Table 1, it appears that our general program is sufficiently accurate for most purposes.

V. MEASUREMENT MATRICES

Any linear measurement of the field from a current $\underset{\sim}{J}$ on a body S can be expressed as a linear functional of $\underset{\sim}{J}$, that is

$$\text{measurement} = \iint_S \underset{\sim}{E}^r \cdot \underset{\sim}{J}\, ds \tag{64}$$

where $\underset{\sim}{E}^r$ is a known function. If the excitation-measurement system is viewed as a two-port system, it can be shown that $\underset{\sim}{E}^r$ in (64) is the field on S when the measurement port is excited.[3] For a moment solution, the current is given by a superposition $\underset{\sim}{J} = \Sigma\, I_j \underset{\sim}{J}_j$, and (64) reduces to

$$\text{measurement} = [R]\,[I] \tag{65}$$

where [I] is the matrix (15) and [R] is a measurement <u>row</u> matrix

$$[R] = [\langle \underset{\sim}{J}_j,\ \underset{\sim}{E}^r \rangle] \tag{66}$$

Note the similarity of [R] to the excitation matrix defined by (14). If the matrix solution (17) is now substituted into (65), one has

$$\text{measurement} = [R][Y][V] \tag{67}$$

The symmetry of (67) with respect to [R] and [V] reflects the reciprocity theorem of electromagnetic theory.

For bodies of revolution, the expansion for $\underset{\sim}{J}$ can be separated into t and ϕ directed components, according to (23). It is then convenient to partition [R] into t and ϕ component terms as

$$(R_n^t)_i = \langle \underline{J}_{ni}^t, \underline{E}^r \rangle$$

$$(R_n^\phi)_i = \langle \underline{J}_{ni}^\phi, \underline{E}^r \rangle \tag{68}$$

The analogous partition for excitation [V] is given by (27). Now one can rewrite (67) in partitioned form as

$$\text{measurement} = \left[[R_n^t] \quad [R_n^\phi] \right] \begin{bmatrix} [Y_n^{tt}] & [Y_n^{t\phi}] \\ [Y_n^{\phi t}] & [Y_n^{\phi\phi}] \end{bmatrix} \begin{bmatrix} [V_n^t] \\ [V_n^\phi] \end{bmatrix} \tag{69}$$

where the Y submatrices are obtained after the Z matrix is inverted, and are not the inverses of the corresponding Z submatrices.

An important special case is that of radiation field measurement. It has been shown that the radiation field from currents $\underline{J}$ on S is given by[8]

$$\underline{E} \cdot \underline{u} = \frac{-j\omega\mu}{4\pi r} e^{-jkr} [R] [I] \tag{70}$$

where the elements of [R] are given by (66) with

$$\underline{E}^r = \underline{u}\, e^{-jk} \cdot \underline{r} \tag{71}$$

This is a unit plane wave with polarization vector $\underline{u}$ and propagation vector $\underline{k}$. An arbitrary plane wave is a superposition of two orthogonal components, say $\underline{E}_\theta$ and $\underline{E}_\phi$. Hence, one can treat the general case as two applications of (71), one for $\underline{u} = \underline{u}_\theta$ and the other for $\underline{u} = \underline{u}_\phi$. To distinguish between the two cases let

$$(R_n^{t\theta})_i = \langle J_{ni}^t, E_\theta^r \rangle$$
$$(R_n^{\phi\theta})_i = \langle J_{ni}^\phi, E_\theta^r \rangle \tag{72}$$

for the θ-polarized case, and

$$(R_n^{t\phi})_i = \langle J_{ni}^t, E_\phi^r \rangle$$
$$(R_n^{\phi\phi})_i = \langle J_{ni}^\phi, E_\phi^r \rangle \tag{73}$$

for the ϕ-polarized case.

The excitation matrices can now be evaluated as follows. Let

$$E_\theta^r = u_\theta^r \, e^{jk(\rho \sin\theta_r \cos\phi + z\cos\theta_r)} \tag{74}$$

where θ_r and $\phi_r = 0$ are the angles to the field point of measurement. The dot products required in (72) are given by

$$u_t \cdot u_\theta^r = \cos\theta_r \sin v \cos\phi - \sin\theta_r \cos v$$
$$u_\phi \cdot u_\theta^r = -\cos\theta_r \sin\phi \tag{75}$$

Using the integral formula for Bessel functions

$$J_n(\rho) = \frac{j^n}{2\pi} \int_0^{2\pi} e^{-j\rho\cos\phi} \, e^{-jn\phi} \, d\phi \tag{76}$$

one can now evaluate the ϕ integrations in (72), obtaining

$$(R_n^{t\theta})_i = 2\pi j^{n+1} \int_0^N dt\, \rho\, f_i(t)\, e^{jkz\cos\theta_r} \left[\cos\theta_r \sin v \frac{J_{n+1}-J_{n-1}}{2} + j \sin\theta_r \cos v \, J_n\right]$$
$$(R_n^{\phi\theta})_i = -2\pi j^{n+1} \int_0^N dt\, \rho\, f_i(t)\, e^{jkz\cos\theta_r} \cos\theta_r \frac{J_{n+1}+J_{n-1}}{2j} \tag{77}$$

where

$$J_n = J_n(k\rho \sin \theta_r) \tag{78}$$

Similarly, to evaluate (73), let

$$\underline{E}_{\phi}^{r} = \underline{u}_{\phi}^{r} \, e^{jk(\rho \sin \theta_r \cos \phi + z \cos \theta_r)} \tag{79}$$

The required dot-products are then

$$\begin{aligned} \underline{u}_t \cdot \underline{u}_{\phi}^{r} &= \sin v \sin \phi \\ \underline{u}_{\phi} \cdot \underline{u}_{\phi}^{r} &= \cos \phi \end{aligned} \tag{80}$$

and the ϕ integrations in (73) can be performed. The result is

$$\begin{aligned} (R_n^{t\phi})_i &= 2\pi j^{n+1} \int_0^N dt \; \rho \, f_i(t) \, e^{jkz \cos \theta_r} \sin v \frac{J_{n+1}+J_{n-1}}{2j} \\ (R_n^{\phi\phi})_i &= 2\pi j^{n+1} \int_0^N dt \; \rho \, f_i(t) \, e^{jkz \cos \theta_r} \; \frac{J_{n+1}-J_{n-1}}{2} \end{aligned} \tag{81}$$

where (78) again applies. For computation, the $\rho \, f_i(t)$ in (77) and (81) were the triangle functions (31). The remaining integrals must be evaluated numerically for bodies of arbitrary contour. In general, $R_n^{t\theta}$ and $R_n^{\phi\phi}$ are even in n, while $R_n^{\phi\theta}$ and $R_n^{t\phi}$ are odd in n. As shown by (22) and (24), the excitation matrix [V] differs from the measurement matrix [R] only by the sign of n. Hence, for plane-wave excitation of the body,

$$(V_n^{pq})_i = (R_{-n}^{pq})_i \tag{82}$$

where pq represents $t\theta$, $\phi\theta$, $t\phi$, or $\phi\phi$. Equation (82) means that the V_i are given by (77) and (81) with n replaced by -n and θ_r by θ_t, and does not imply equality of excitation and measurement.

For axial incidence of plane waves, equations (77) and (81) reduce considerably. In this case $\theta_r = \pi$ and all $R_n = 0$ except

$$
\begin{aligned}
(R_1^{t\theta})_i &= (R_{-1}^{t\theta})_i = -\pi \int_0^N dt\ \rho\ f_i(t)\ e^{-jkz} \sin v \\
(R_1^{\phi\theta})_i &= -(R_{-1}^{\phi\theta})_i = j\pi \int_0^N dt\ \rho\ f_i(t)\ e^{-jkz} \\
(R_1^{t\phi})_i &= -(R_{-1}^{t\phi})_i = -j(R_1^{t\theta})_i \\
(R_1^{\phi\phi})_i &= (R_{-1}^{\phi\phi})_i = -j(R_1^{\phi\theta})_i
\end{aligned}
\tag{83}
$$

Hence, only the n = -1 and n = +1 modes are excited by axially incident plane waves.

VI. APERTURE ANTENNAS

An aperture antenna is a radiating system consisting of a conducting body with apertures through which electromagnetic energy is supplied. For analysis purposes, it is assumed that the tangential electric field $\underset{\sim}{E}_t$ is known over the aperture. It is, of course, zero over the conducting body. This known field $\underset{\sim}{E}_t$ corresponds to $\underset{\sim}{E}_t^s = -\underset{\sim}{E}_t^i$ in the general analysis of Section I. Figure 3 represents the general problem, showing the body S, the aperture, and radius vector to a distant field point.

In terms of a moment solution, the excitation is the known $\underset{\sim}{E}_t$ in the aperture, from which the excitation matrix may be computed by (14) by setting $\underset{\sim}{E}^i = -\underset{\sim}{E}_t$. In general, this results in an excitation of many $e^{jn\phi}$ modes, each of which can be treated separately. The current on S for each mode is found by inverting (25), and the total current is the sum of the modal currents, that is

$$\underset{\sim}{J} = \sum_n [\underset{\sim}{J}_n] [Y_n] [V_n] \tag{84}$$

where n denotes the mode. Similarly, the radiation field for each mode is found from (70), and the total radiation field is the sum of the modal fields, that is

$$E_u = \frac{-j\omega\mu}{4\pi r} e^{-jkr} \sum_n [R_n] [Y_n] [V_n] \tag{85}$$

where u = θ or ϕ, and n again denotes the mode.

For simplicity, illustrative computations have been made only for the case of excitation independent of ϕ, which excites only the n = 0 mode.

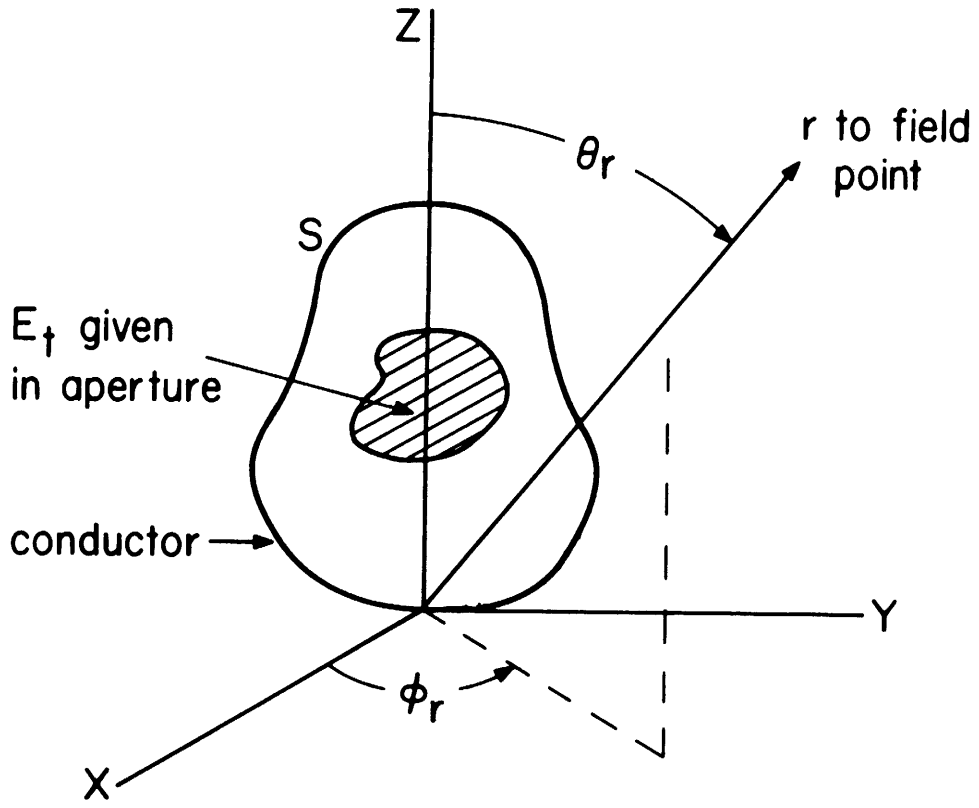

Figure 3. An aperture in a conducting body of revolution.

This results in a further simplification in that $[Z_0^{t\phi}] = [Z_0^{\phi t}] = 0$, that is, there is no coupling between the t-directed currents and the ϕ-directed currents. From symmetry considerations, an excitation having only an E_t component produces only a J_t current, and an excitation having only an E_ϕ component produces only a J_ϕ current. Hence, the problem reduces to two independent ones,

$$J_t = [J_0^t][Y_0^{tt}]\,[V_0^t]$$
$$J_\phi = [J_0^\phi]\,[Y_0^{\phi\phi}]\,[V_0^\phi] \tag{86}$$

for the current, and

$$E_\theta = \frac{-j\omega\mu}{4\pi r} e^{-jkr}\,[R_0^{t\theta}]\,[Y_0^{tt}]\,[V_0^t]$$
$$E_\phi = \frac{-j\omega\mu}{4\pi r} e^{-jkr}\,[R_0^{\phi\phi}]\,[Y_0^{\phi\phi}]\,[V_0^\phi] \tag{87}$$

for the radiation field. The $[Y_0^{tt}]$ and $[Y_0^{\phi\phi}]$ in (86) and (87) are the inverses of $[Z_0^{tt}]$ and $[Z_0^{\phi\phi}]$, respectively.

To check the program, radiation from an equatorially slotted conducting sphere was computed both by the classical eigenfunction expansion and by the general program. Figure 4 shows the current density on a sphere of radius $a = 0.2\lambda$ excited by an $E_\theta = \delta(\theta-\pi/2)/a$ in the equatorial slot. This gives rise to $V_{0j}^{t\theta} = 2\pi$ if t_j is on the equator, and zero otherwise. The eigenfunction solution was computed using 18 terms of the Fourier series. The real part of the current converged very rapidly, and can be considered as exact. The imaginary part of the current does not converge at the source, and converges

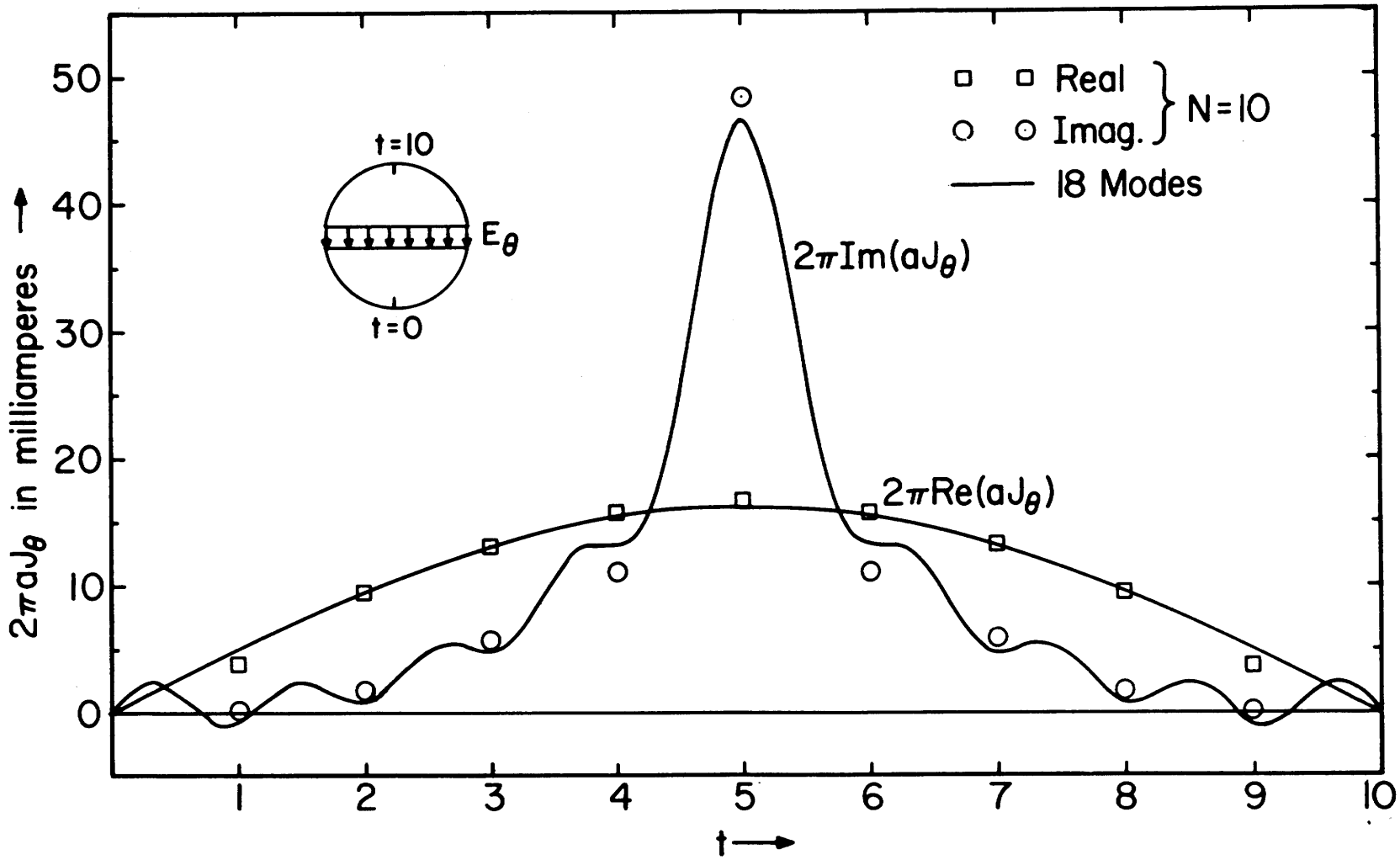

Figure 4. Current density on a conducting sphere of radius 0.2λ, excited by one volt across an equatorial slot.

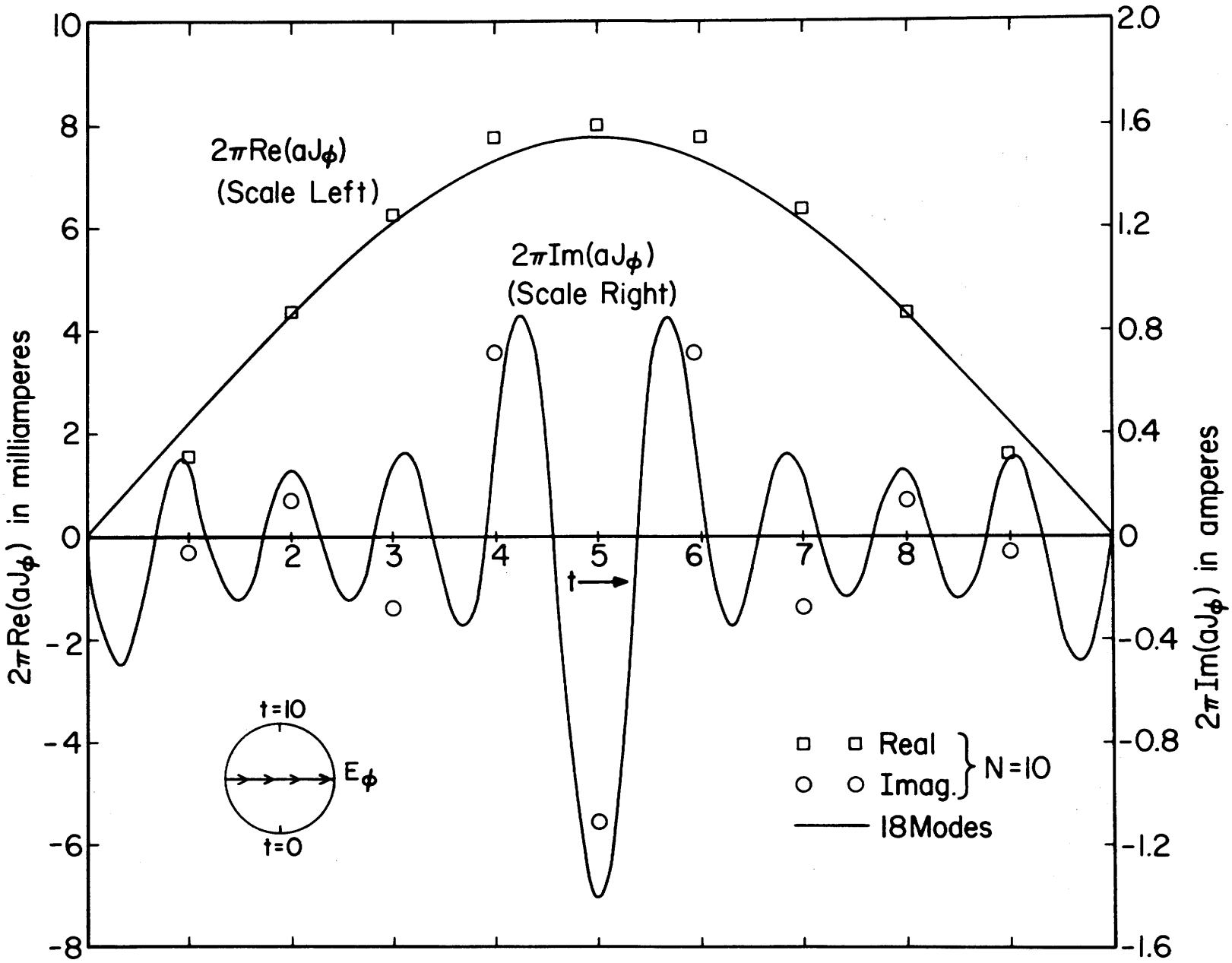

Figure 5. Current density on a conducting sphere of radius 0.2λ, excited by an impulsive E_ϕ in an equatorial slot.

slowly elsewhere, and hence the imaginary part computed from 18 terms of the Fourier series is not exact. As can be seen in Figure 4, the N = 10 solution using the general program is in good agreement with the eigenfunction solution. Computation of radiation field patterns for the two solutions agreed to within less than one percent accuracy, and hence are not shown.

Figure 5 shows the current density on a sphere of radius a = 0.2λ excited by an $E_\phi = -\delta(\theta-\pi/2)/a$ in the equatorial slot. This gives rise to $V_{oj}^{\phi\phi} = 2\pi$ when t_j is on the equation, and zero otherwise. Again the eigenfunction solution was computed using 18 terms of the Fourier series, and the real part of the current converged very rapidly. However, the imaginary part of the current does not converge. The real part of the current computed from the N = 10 case of the general program again agrees well with the eigenfunction solution. It is difficult to say anything about the imaginary part because of the divergent nature of the solution. Computation of the radiation field patterns for the two solutions again agreed to within a few percent. Evidently the radiation pattern does not depend strongly on the non-converging imaginary part of the current.

As an example of a body of more complicated shape, computations were made for aperture excitation of a cone-sphere. This body is formed by wedging a conducting sphere into a conducting cone, resulting in a shape similar to that of an ice cream cone. The radius of the sphere is a = 0.2λ, and the cone half angle is 10°. The aperture is a narrow slot near the cone-to-sphere junction. Figure 6 shows the current density when the excitation is an impulsive E_t in the slot. An N = 20 solution is shown, but smaller values of N give reasonably accurate solutions.

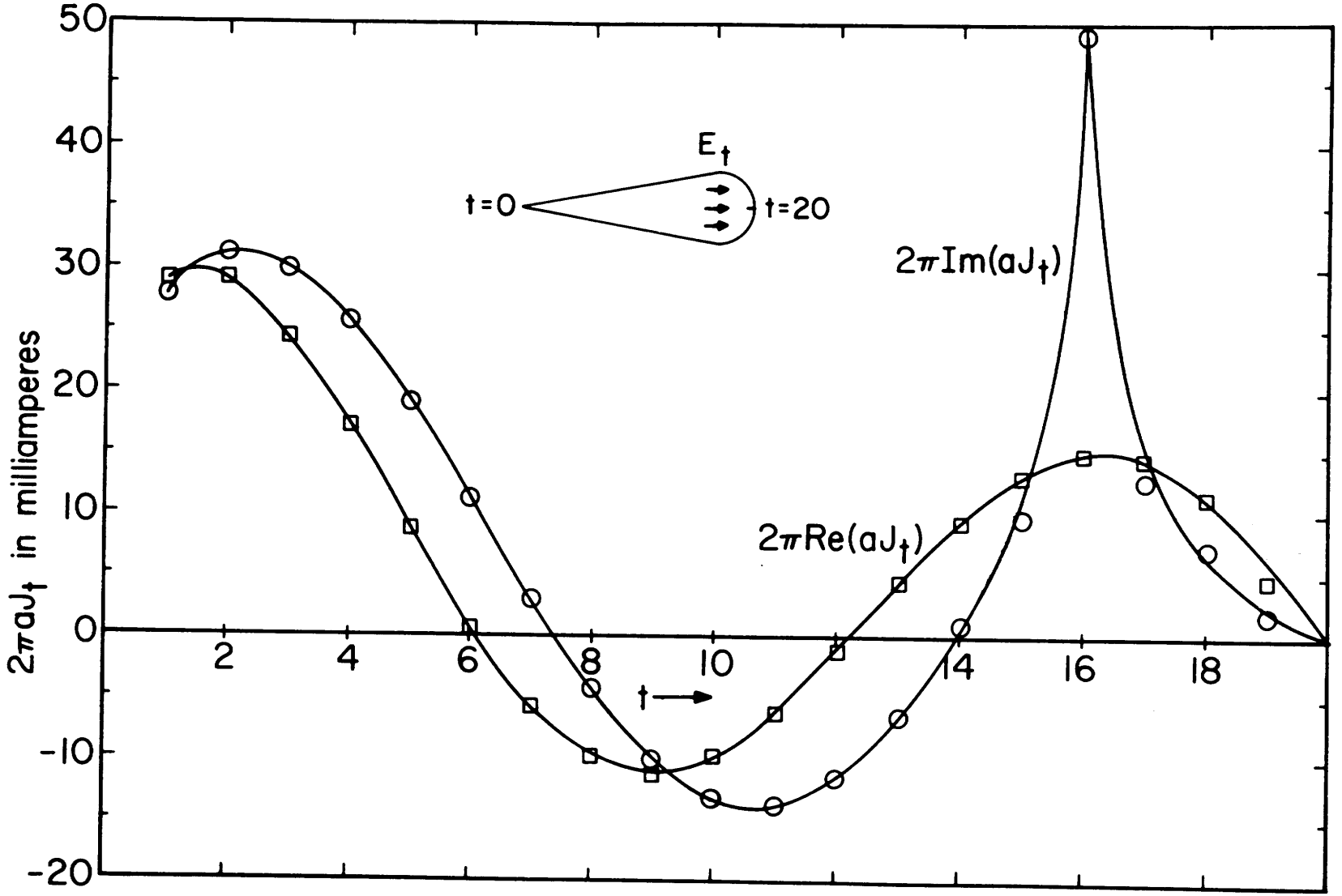

Figure 6. Current density on a conducting cone-sphere excited by one volt across a slot at the cone-to-sphere junction.

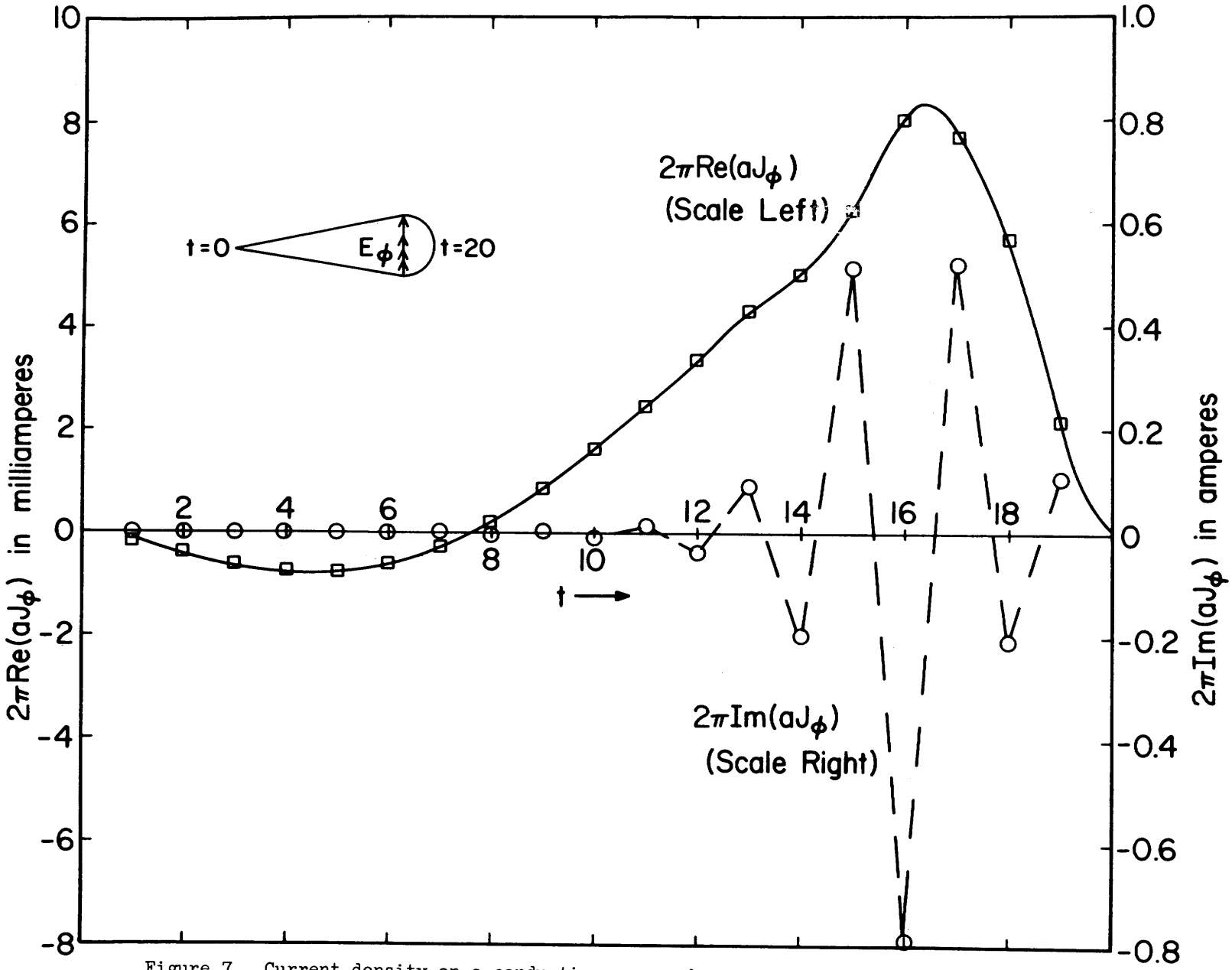

Figure 7. Current density on a conducting cone-sphere excited by an impulsive E_{ϕ} in a slot at the cone-to-sphere junction.

Figure 7 shows the same cone-sphere excited by an impulsive E_ϕ in the slot. Again an N = 20 solution is shown, but usable results could be obtained with a smaller N. Note the extreme oscillatory nature of the imaginary part of the current. Theoretically, the imaginary part does not converge, as discussed previously for the sphere.

Figures 8 and 9 show the power gain patterns for the two cone-sphere excitations discussed above. For a given polarization, the power gain normalized to omnidirectional radiation is[9]

$$g_u = \frac{4\pi r^2 |E_u|^2}{\eta\, P_{rad}} \tag{88}$$

where $\eta = \sqrt{\mu/\epsilon}$ and P_{rad} is the power radiated. From (70) and (17), the numerator of (88) can be expressed as

$$4\pi r^2\, |E_u|^2 = \frac{1}{4\pi}\left| k\eta\, [R]\, [Y]\, [V] \right|^2 \tag{89}$$

In general, the power radiated is given by[10]

$$P_{rad} = -\mathrm{Re} \oint\!\!\oint_S \underline{E}^* \cdot \underline{J}\, ds = \mathrm{Re}\, [\hat{V}]\, [Y]\, [V] \tag{90}$$

where the elements of the row matrix $[\hat{V}]$ are

$$\hat{V}_i = - \oint\!\!\oint_S \underline{E}^* \cdot \underline{J}_i\, ds \tag{91}$$

For the excitations used in Figures 8 and 9, only one V_i is nonzero, and $V_i = \hat{V}_i = 2\pi$. Hence (90) reduces to a single element of the [Y] matrix. In

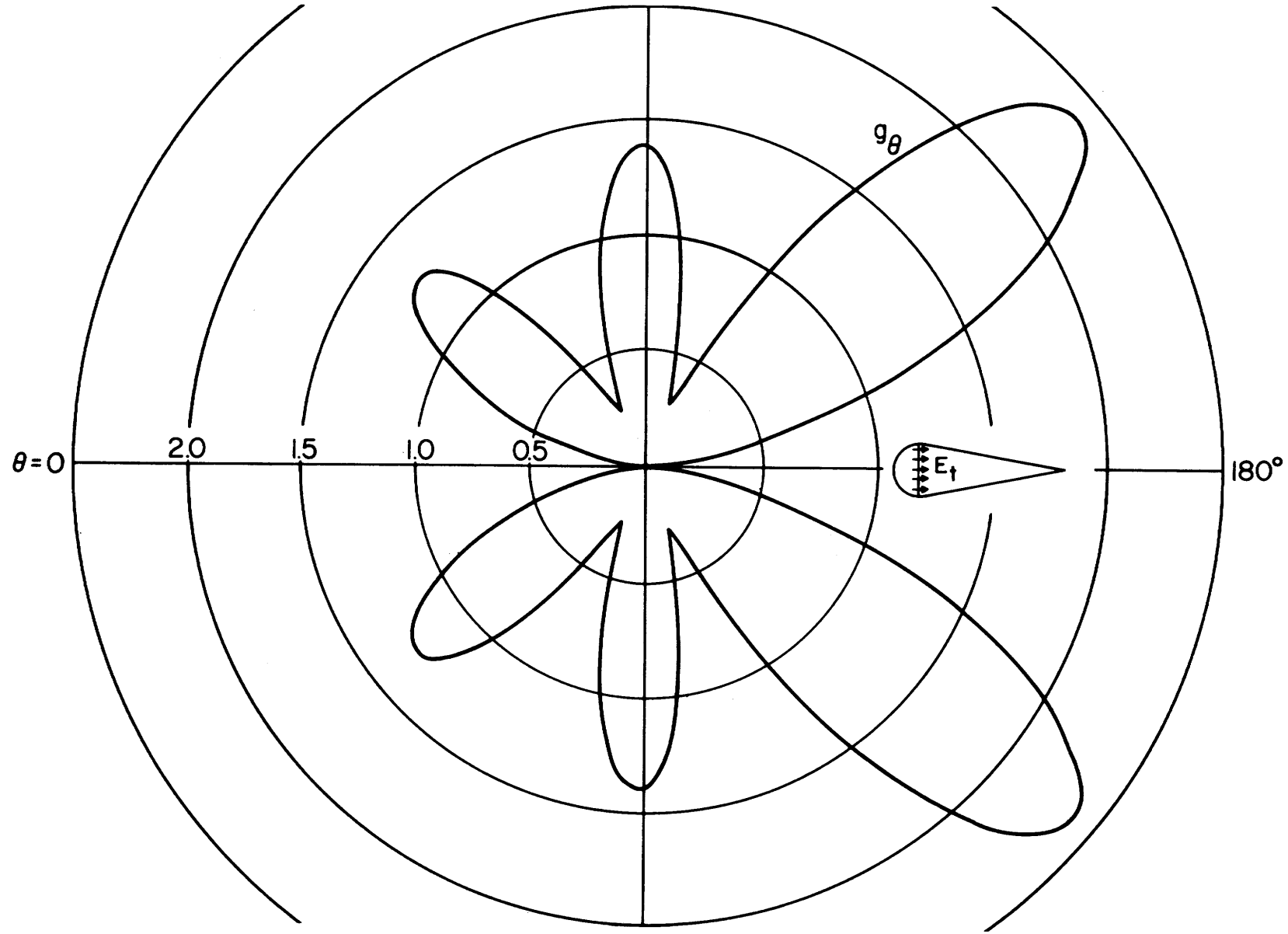

Figure 8. Power gain pattern for radiation from a conducting cone-sphere excited by one volt across a slot at the cone-to-sphere junction.

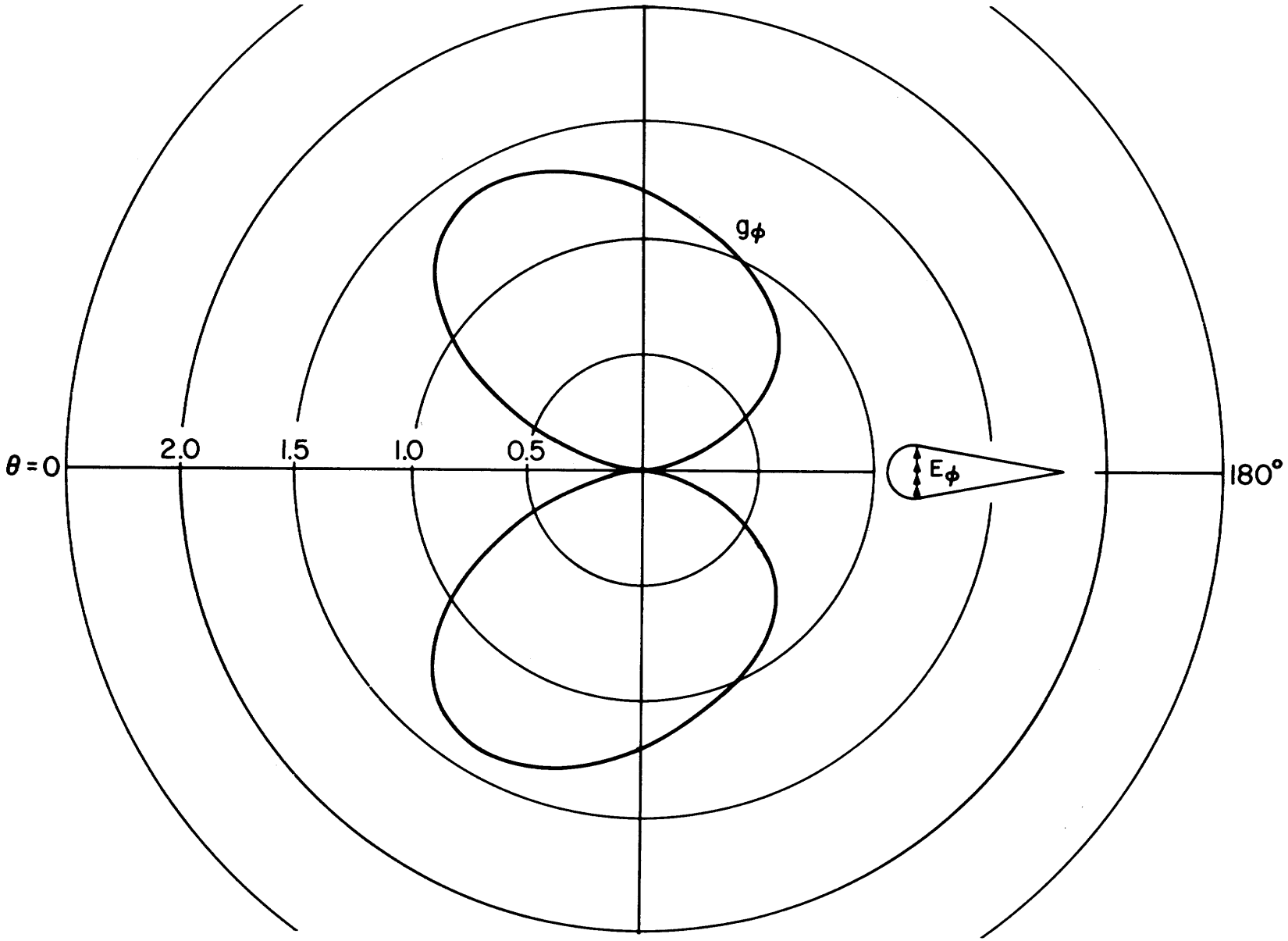

Figure 9. Power gain pattern for radiation from a conducting cone-sphere excited by an impulsive E_ϕ in a slot at the cone-to-sphere junction.

particular, for Figure 8,

$$g_{\theta} = \frac{\eta k^2 \left| \sum_{j=1}^{N-1} (R_n^{t\theta})_j \, (Y_n^{tt})_{ji} \right|^2}{4\pi \, \mathrm{Re}(Y_n^{\theta\theta})_{ii}} \tag{92}$$

where t_i is the point of excitation. Similarly, for Figure 9,

$$g_{\phi} = \frac{\eta k^2 \left| \sum_{j=1}^{N-1} (R_n^{\phi\phi})_j \, (Y_n^{\phi\phi})_{ni} \right|^2}{4\pi \, \mathrm{Re}(Y_n^{\phi\phi})_{ii}} \tag{93}$$

where again t_i is the point of excitation.

VII. PLANE-WAVE SCATTERING

The radar scattering problem consists of a plane wave incident on a scattering body, plus measurement of the far-zone scattered field. Figure 10 illustrates the geometry of the problem for conducting bodies of revolution. In general, the incident wave $\underline{E}^i$ can be expressed as a superposition of the two orthogonal components E^i_θ and E^i_ϕ, and similarly the far-zone scattered wave $\underline{E}^s$ as the superposition of E^s_θ and E^s_ϕ. These are related by the scattering matrix [s] of the body according to

$$\begin{bmatrix} E^s_\theta \\ E^s_\phi \end{bmatrix} = \frac{e^{-jkr}}{r} \begin{bmatrix} s^{\theta\theta} & s^{\theta\phi} \\ s^{\phi\theta} & s^{\phi\phi} \end{bmatrix} \begin{bmatrix} E^i_\theta \\ E^i_\phi \end{bmatrix} \tag{94}$$

The elements of [s] can be expressed as a summation over the modal components

$$s^{pq} = \sum_n s^{pq}_n \tag{95}$$

where pq denotes $\theta\theta$, $\theta\phi$, $\phi\theta$, or $\phi\phi$. The scattered field is given by (70), and hence

$$s^{pq}_n = \frac{-j\omega\mu}{4\pi} \begin{bmatrix} [R^{tp}_n] & [R^{\phi p}_n] \end{bmatrix} \begin{bmatrix} [Y^{tt}_n] & [Y^{t\phi}_n] \\ [Y^{\phi t}_n] & [Y^{\phi\phi}_n] \end{bmatrix} \begin{bmatrix} [V^{tq}_n] \\ [V^{\phi q}_n] \end{bmatrix} \tag{96}$$

where the R_n elements are given by (77) or (81), and the V_n elements by the

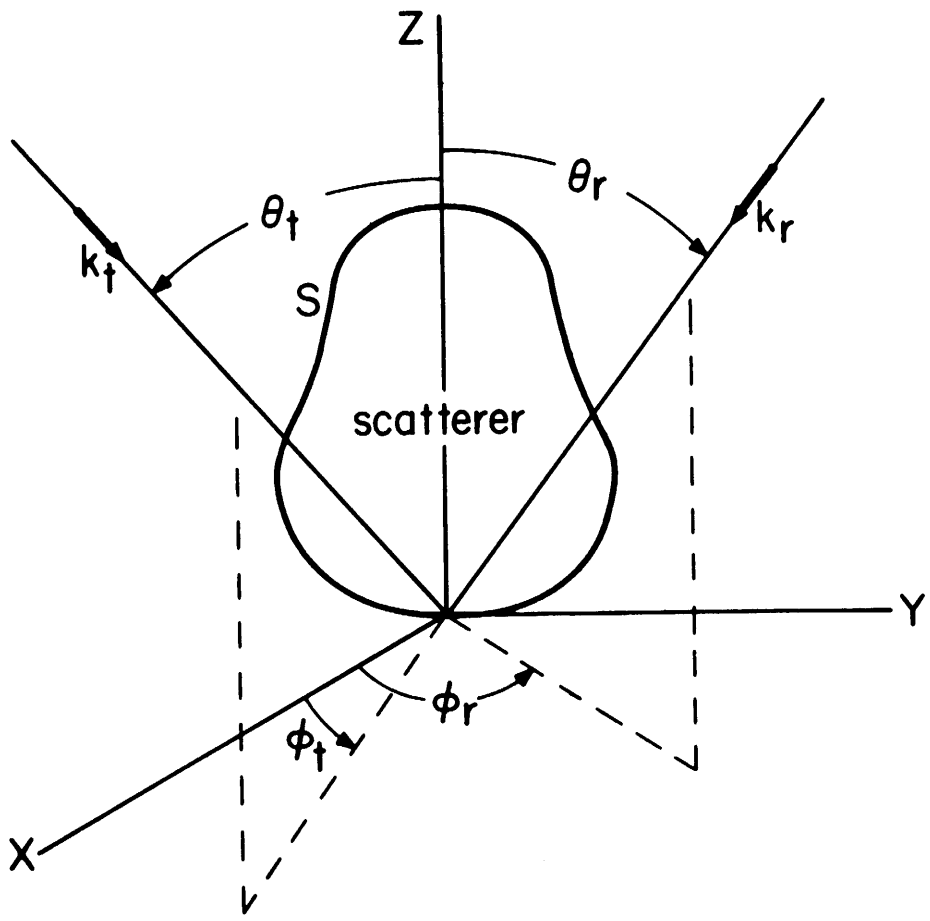

Figure 10. Plane-wave scattering by a conducting body of revolution.

same formulas with n replaced by -n and θ_r by θ_t.

Radar scattering data are often presented in terms of the radar cross section, defined as

$$\sigma^{pq} = 4\pi r^2 \left| \frac{E_p^s}{E_q^i} \right|^2 \tag{97}$$

As indicated, σ depends both on the received polarization p and the incident polarization q. It follows from (94) and (97) that for a given polarization,

$$\sigma^{pq} = 4\pi |s^{pq}|^2 \tag{98}$$

An incident wave of arbitrary polarization can be expressed as the superposition

$$\underline{E}^i = (\underline{u}_\theta \alpha_\theta + \underline{u}_\phi \alpha_\phi) E^i \tag{99}$$

where $|\alpha_\theta|^2 + |\alpha_\phi|^2 = 1$. The matrix

$$[\alpha] = \begin{bmatrix} \alpha_\theta \\ \alpha_\phi \end{bmatrix} \tag{100}$$

is called the polarization matrix. Let $[\alpha^t]$ be the polarization matrix of the incident wave when the transmitting antenna is excited, and $[\alpha^r]$ be the transpose of the polarization matrix of the incident wave when the receiving antenna is excited. Then the component of scattered field that is polarization-matched to the receiver is

$$E^s = \frac{e^{-jkr}}{r} [\alpha^r] [s] [\alpha^t] E^i \tag{101}$$

and the radar cross section is

$$\sigma = 4\pi \left| [\alpha^r]\ [s]\ [\alpha^t] \right|^2 \tag{102}$$

where [s] is given by (94). Equation (98) is a special case of (102).

For simplicity, only excitation by axially incident plane waves is considered for computation. Let

$$\underline{E}^i = -\underline{u}_x\ e^{-jkz} \tag{103}$$

which can be considered a θ-polarized plane wave from a transmitter at coordinates $\theta_t = \pi$, $\phi_t = 0$. The excitation matrix elements are thus given by the first two equations of (83) with R replaced by V, n by -n, and θ_r by θ_t. Only the $n = \pm 1$ modes are present in the excitation, giving rise to only the same two modes in the current. The symmetry relationships (29) and (82) can now be used to obtain the simpler form

$$\underline{J} = \underline{u}_t J^t \cos\phi + \underline{u}_\phi J^\phi \sin\phi \tag{104}$$

where

$$\begin{aligned} J^t &= 2 \sum_{i=1}^{N-1} (I_1^t)_i\ f_i(\rho) \\ J^\phi &= 2j \sum_{i=1}^{N-1} (I_1^\phi)_i\ f_i(\rho) \end{aligned} \tag{105}$$

and $f_i(\rho) = T(t-t_i)/\rho$. Hence, the current is completely specified by its n = 1 mode coefficients.

To check the program, the current on a sphere excited by the plane wave (103) was computed both by the classical eigenfunction method and by the general computer program. Figure 11 shows the magnitudes of J^t and J^ϕ of (104)

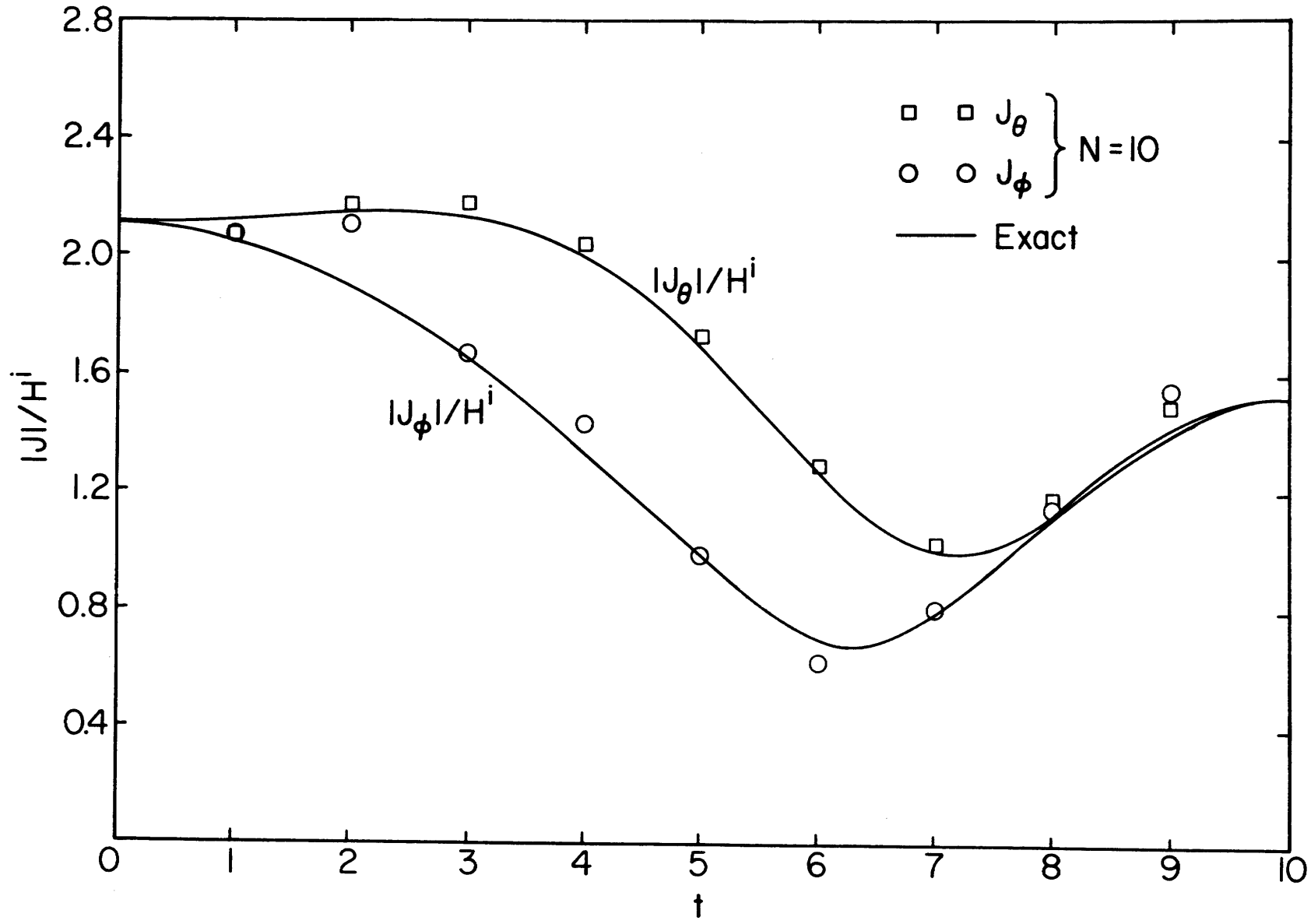

Figure 11. Current density on a conducting sphere of radius 0.2λ excited by a uniform plane wave.

for a sphere of radius a = 0.2λ, using N = 10 for the general program. The eigenfunction expansion converges very rapidly and can be considered as exact. The current density is normalized with respect to the incident magnetic field intensity, giving a dimensionless quantity which is 2 for a plane conductor covering the z = 0 plane. The radar scattering patterns computed by the eigenfunction method and by the N = 10 general solution were almost identical, and are not shown.

Figure 12 shows the current on a cone-sphere excited by a plane wave axially incident on the tip. The radius of the sphere is again 0.2λ, which is the same as used in the antenna examples. Again J^t and J^ϕ of (104), normalized with respect to H^i, are plotted. To illustrate convergence, both the N = 20 (circles) and the N = 30 (solid line) solutions are plotted. The J^t current converges fairly rapidly, but the J^ϕ current converges more slowly. Even the N = 30 solution cannot be considered accurate for J^ϕ. Apparently the rate of convergence is affected by the sharp tip of the cone. For better convergence one could include a term in the current expansion to properly represent the singularity at the tip. However, radar scattering patterns are insensitive to small oscillations in the currents, and more accurate solutions are not needed in most cases.

Figure 13 shows the current on the same cone-sphere excited by a plane-wave axially incident on the spherical end, that is, the end opposite to the point. The above comments concerning convergence apply also to this excitation.

Figures 14 and 15 show radar cross section patterns for the cone-sphere excitations corresponding to Figures 12 and 13, respectively. The plots were made using the N = 20 solution, but the corresponding N = 30 solution gave almost identical results. The only difference occurred in the vicinity of

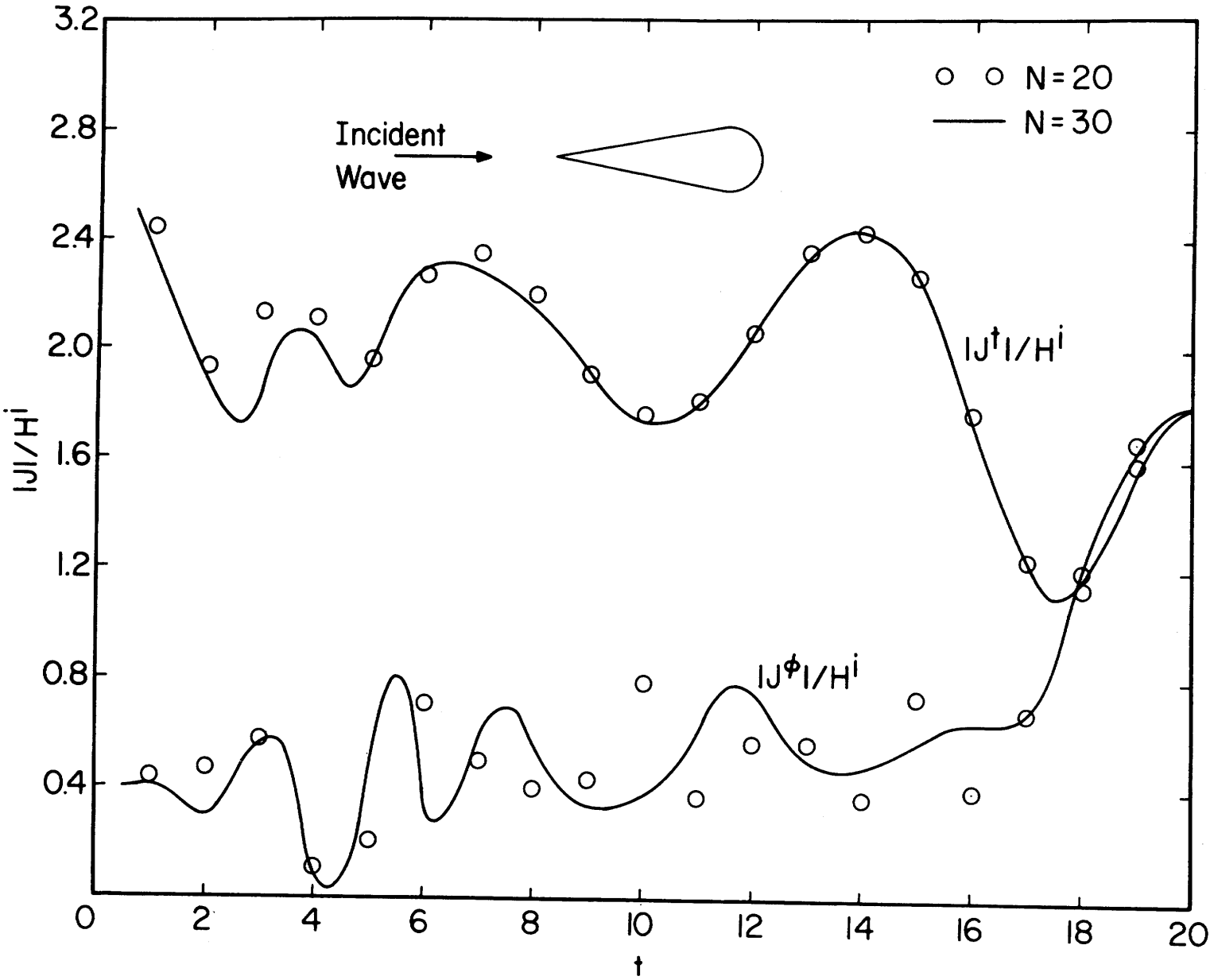

Figure 12. Current density on a conducting cone-sphere (cone angle 20°, sphere radius 0.2λ) excited by a uniform plane wave axially incident on the tip.

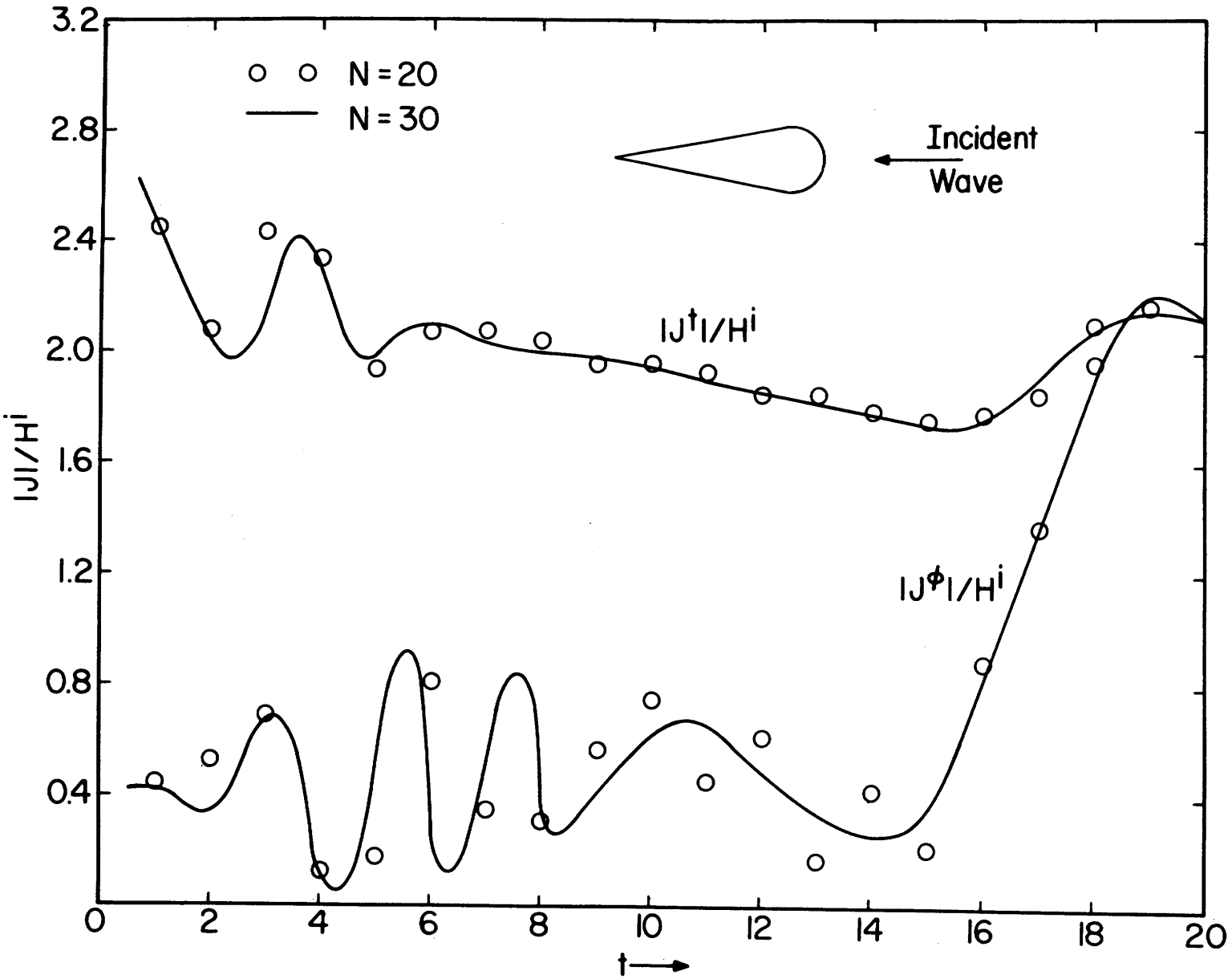

Figure 13. Current density on a conducting cone-sphere (cone angle 20°, sphere radius 0.2λ) excited by a uniform plane wave axially incident on the sphere.

forward scattering where a change in σ of the order of a few percent was obtained. This region is most sensitive to inaccuracies because all parts tend to radiate in phase in the forward direction. All plots are normalized to λ^2 to make them dependent only on length/wavelength dimensions, not on absolute dimensions. The curves labeled $\sigma^{\theta\theta}/\lambda^2$ are in the $\phi = 0$ plane, and are the radar cross sections measured by a θ-polarized receiver. The curves labeled $\sigma^{\phi\theta}/\lambda^2$ are in the $\phi = \pi/2$ plane, and are the radar cross sections measured by a φ-polarized receiver.

Because only the n = 1 and n = -1 modes are present in the excitation, these are the only modes present in the scattered field. From (95) and the symmetry relationships (29) and (82) one can show that

$$s^{\theta\theta} = 2s_1^{\theta\theta} \cos \phi_r$$
$$s^{\phi\theta} = 2j\, s_1^{\phi\theta} \sin \phi_r \tag{106}$$

where $s_1^{\theta\theta}$ and $s_1^{\phi\theta}$ are the n = 1 modal solutions evaluated at $\phi_r = 0$. Hence, from (98) and (106) it follows that the radar cross sections are given by

$$\sigma^{\theta\theta} = 16\pi \left| s_1^{\theta\theta} \right|^2 \cos^2 \phi_r$$
$$\sigma^{\phi\theta} = 16\pi \left| s_1^{\phi\theta} \right|^2 \sin^2 \phi_r \tag{107}$$

Hence, the graphs of Figures 14 and 15 are proportional to the coefficients of $\cos^2 \phi_r$ and $\sin^2 \phi_r$ in (107).

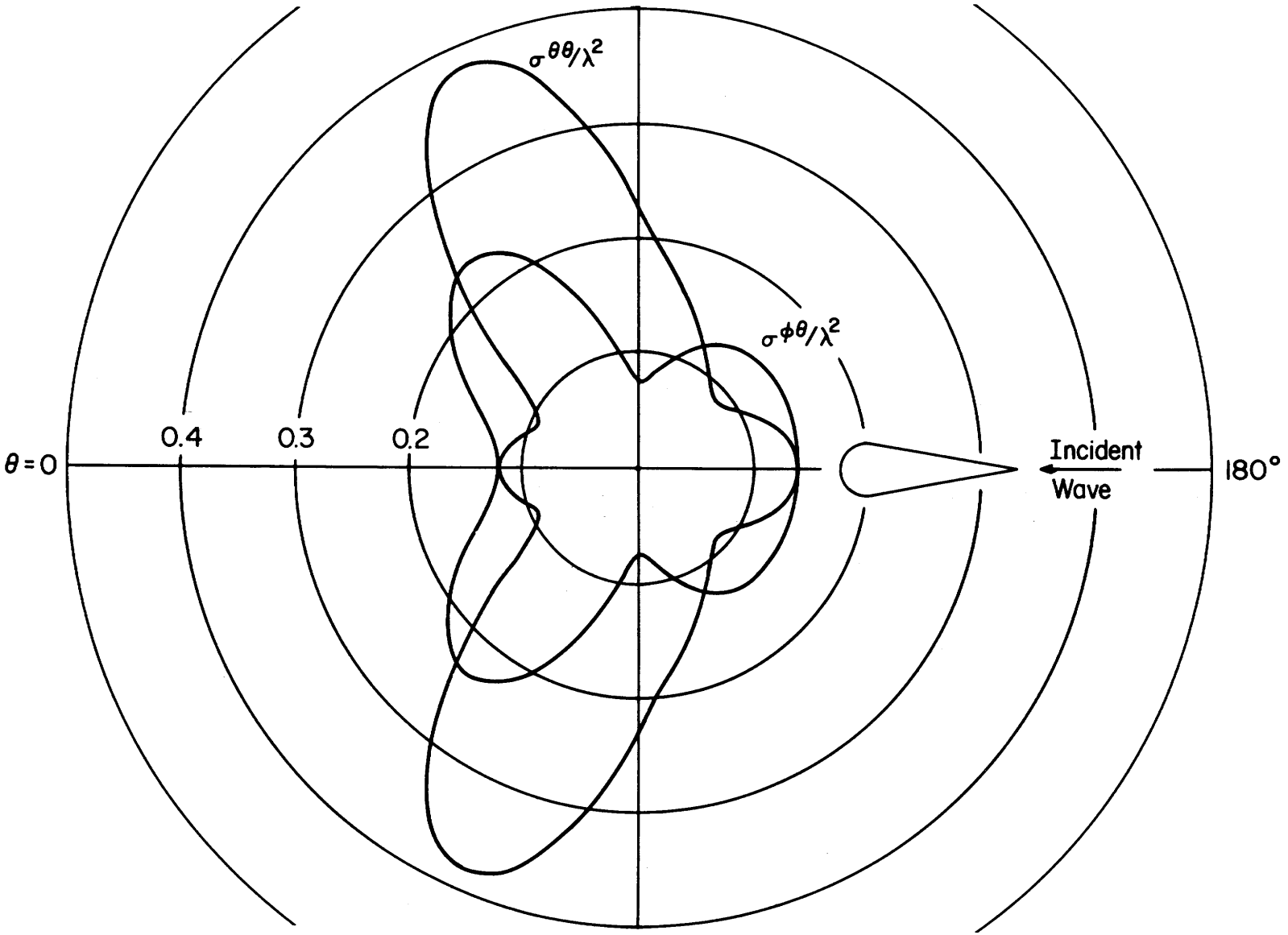

Figure 14. Bistatic scattering cross section for conducting cone-sphere (cone angle 20°, sphere radius 0.2λ) excited by a uniform plane wave axially incident on the tip. $\sigma^{\theta\theta}$ is in the plane $\phi = 0$, and $\sigma^{\phi\theta}$ is in the plane $\phi = \pi/2$.

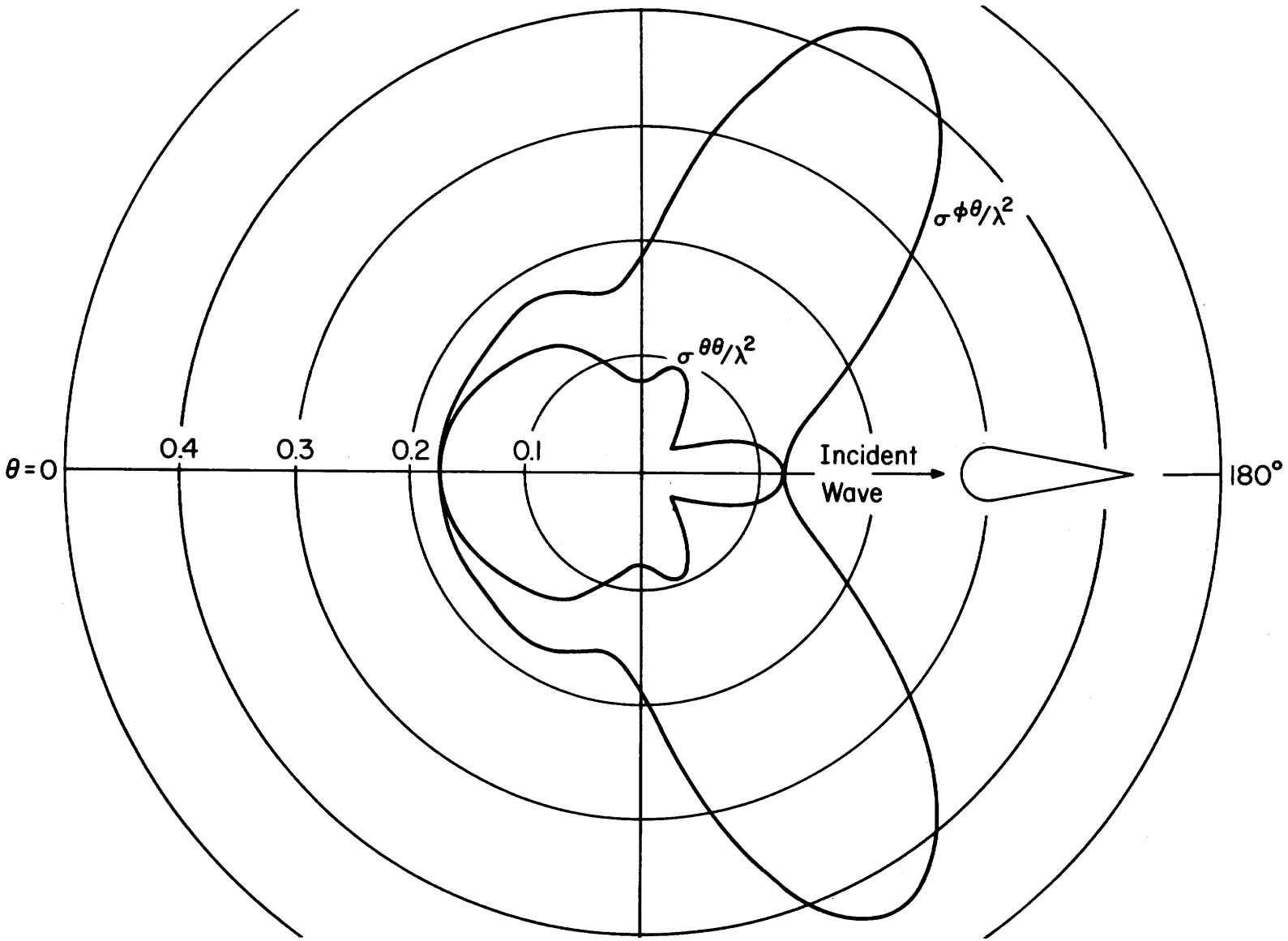

Figure 15. Bistatic scattering cross section for a conducting cone-sphere (cone angle 20°, sphere radius 0.2λ) excited by a uniform plane wave axially incident on the sphere. $\sigma^{\theta\theta}$ is in the plane $\phi = 0$, and $\sigma^{\phi\theta}$ is in the plane $\phi = \pi/2$.

VIII. DISCUSSION

This report develops a solution for the electromagnetic behavior of conducting bodies of revolution with arbitrary excitation in terms of generalized network parameters.[3] Basically, this involves the application of a moment method to the superposition integral representation of the problem. Because of the rotational symmetry, a Fourier series expansion on ϕ is used. To facilitate the handling of arbitrary body contours, a subsectional expansion on t is used. The simplest subsectional function is the pulse function, but it is not in the domain of the original operator because derivatives must be taken. The derivative can be replaced by a finite difference approximation, thereby approximating the operator. However, it was found that difference approximations did not yield as good accuracy as desired. The next simplest subsectional function is the triangle function, and this was used for the general program. Its derivative is a doublet pulse, and hence no approximation of the operator is necessary.

Three types of singularities are encountered in the general solution: (a) a singularity in the coordinate system along the z axis, (b) singularities of curvature in the body contour, such as at a cone tip, and (c) singularities in the excitation. The first type introduces difficulties in the numerical evaluation of the impedance elements, but can be overcome by careful analysis. The second type could be taken care of by special subroutines at points of discontinuity in body curvature, but would be difficult to implement. No attempt has been made to do this in the general program. The third type of singularity is impractical to include in a general solution, because then the

impedance matrix would depend on the excitation instead of being a function of the body geometry alone. It could, however, be incorporated into particular solutions. For example, the singularity in the current at feed point of a slot-fed antenna can be accounted for by including the proper singularity in the expansion functions.

If only the radiation and scattering patterns are wanted, but not the current, then less accuracy is required in the solution. This is because such patterns are continuous linear functionals of the current, and, as shown by the calculus of variations, are accurate to the second order when the currents are accurate to the first order. For example, if the current has an error of the order of ten percent, the radiation field has an error of the order of only one percent. Furthermore, the radiation depends primarily on the current moment ρJ instead of the current itself. Hence, inaccuracies at the poles ($\rho = 0$) of the body have little effect on the radiation pattern. Finally, rapid oscillations in the current about the correct value also have little effect on the radiation field. They contribute mainly to near-field stored energy.

The generalized network parameters of a body are basically a matrix approximation to the functional operator equation for the problem. Hence, so long as the computational approximations are valid, one can compute the response of the body to arbitrary electromagnetic excitation. Aperture antennas (Section VI) and plane-wave scattering (Section VII) are but two examples. Another problem of interest is excitation by current dipoles in the vicinity of the body. Still more generally, both the excitation and measurement can be taken in the near-zone if desired. Radiation by loaded aperture antennas and scattering by loaded scattering antennas can also be

treated by known methods.[4,11]

Other problems can be treated by modifications or extensions of the theory. For example, the internal resonances of a cavity of revolution can be found by a procedure similar to that used for waveguides of arbitrary cross section.[12] The problem of scattering by a homogeneous dielectric or magnetic body of revolution can be treated in terms of equivalent electric and magnetic surface currents. Hence, an extension to include both electric and magnetic currents could be used to solve such problems.

APPENDIX A

THE COMPUTER PROGRAM

This appendix provides a description, in terms of Fortran IV language, of the computer program that finds the generalized impedance and admittance matrices for a conducting body of revolution with surface S. Section A-1 gives instructions for using the computer program while Section A-2 gives some explanatory notes to facilitate possible modifications. Section A-3 lists the computer program along with the data for the first mode (n=1 in (45)) of a sphere of radius $10/\pi$ and radius to wavelength ratio 0.2. Section A-4 gives the printed output for this same data.

A-1 Instructions for using the computer program

The program, written in Fortran IV level G and tested on an IBM System/360 model 50 computer, accepts punched card input data and outputs the generalized impedance and admittance matrices via both the printed line and a direct access storage device.

The direct access storage device was assigned the data set reference number 4. Statement number 1 early in the main program

```
1 REWIND 4
```

returns the data set number 4 to the first record if it is not already there. Each unformated WRITE (4) statement defines a new record on data set number 4. If the first n records have been written previously, it may be desirable to skip them and start writing on the (n+1) record. This is effected by following statement 1 with n identical READ (4) statements. There are no such READ (4) statements in the listing of the program in Section A-3.

All the punched card data are read early in the main program according to the statements

```
50 READ (1,51,END=52) NN, N, NPHI, BK
51 FORMAT (3I3,E14.7)
   KG = 2*N
61 READ (1,53)(VS(J), J = 1,KG)
62 READ (1,53)(ZS(J), J = 1, KG)
63 READ (1,53)(R(J), J = 1, KG)
53 FORMAT (10F8.4)
```

in that order. According to statement 50, several sets of data may be processed with control going to statement 52 when the data are exhausted. Statement 52 is a stop.

NN = the mode number the same as n appearing in (45). NN must be either zero or a positive integer. If NN is large, NPHI must also be large for the numerical integration (46) to be accurate.

N = total length of the generating curve. N is a positive integer. There will be N-1 expansion functions for the t directed current and N-1 expansion functions for the ϕ directed current. Consequently, the Z and Y matrices will be 2*(N-1) by 2*(N-1). For N larger than 20, present dimension statements must be altered.

NPHI = the number of equal subdivisions of the ϕ axis from 0° to 180°. NPHI corresponds to the positive integer M appearing in (46). NPHI must be large enough so that $\frac{\pi}{\text{NPHI}} * \text{NN}$ is less than a radian. The maximum electrical length corresponding to an excursion $\frac{\pi}{\text{NPHI}}$ in

ϕ should also be less than a radian. If NPHI is larger than 40, present dimension statements must be altered.

BK = propagation constant k appearing in (46). For reliable results, BK should be less than one.

VS(J), ZS(J) and R(J) are arrays that describe the geometry of the surface S of revolution. The J indicates evaluation at $t = \frac{J-.5}{2}$, where t is the arc length along the generating curve, zero at the lower pole of the body of revolution. J runs from 1 to 2*N.

VS = the angle (radians) between $\underset{\sim}{u}_t$ the unit vector in the t direction and the axis (z axis) of the body of revolution. VS is positive when $\underset{\sim}{u}_t$ is diverging from the z axis and negative otherwise.

ZS = axial distance z from the lower pole

R = distance ρ from the z axis.

All of the above data are printed after they are read in. Statement 58

```
58 WRITE (3,64)(G(K), K = 1, NG)
```

prints some G_n's of equation (52). The Z matrix is printed by

```
95 WRITE (3,88)(Z(K), K = K1,K2)
88 FORMAT (1X, 12G11.4)
```

inside DO loops 89 and 90. The impedance matrix is stored columnwise in the linear array Z. The submatrix $(Z_n^{tt})_{ij}$ of (45) is labeled Z1 and printed columnwise. The first element of each column begins a new line. For a column of the submatrix $(Z_n^{tt})_{ij}$ the "source point" j is fixed and the "field point" i runs from the lower pole to the upper pole. Similarly, $Z^{\phi t}$, $Z^{t\phi}$ and

$Z^{\phi\phi}$ are labeled Z2, Z3, and Z4 and printed. The impedance matrix is put into direct access storage by

```
33 WRITE (4)(Z(I), I = 1, NZ)
```

Next, the admittance matrix (inverse of the impedance matrix) is calculated and put into the same array Z. The admittance matrix is outputed exactly as the impedance matrix was. The printing is by

```
96 WRITE (3,88)(Z(K), K = K1,K2)
```

in DO loops 93 and 92. The direct access data set 4 is written by

```
34 WRITE (4)(Z(I), I = 1, NZ)
```

Throughout the program, the sequence

```
CALL CLOCK (I1,I2)
WRITE (3,99) I1,I2
99 FORMAT (1X,2I7)
```

appears many times. CLOCK is a subroutine which, perhaps not available on all 360 computers, can be called as easily as SIN or COS. The first argument I1 becomes the time in seconds while the second one I2 gives the year and day.

A-2 Explanatory notes on the computer program.

LINEQ(LL,C), the first subroutine to be compiled, accepts an LL by LL complex matrix stored columnwise in the linear complex array C and returns the inverse of this LL by LL matrix into the same array C. Of course, the original elements of the matrix are destroyed. Although the dummy array C is only

dimensioned C(1) in the subprogram, all the space of the corresponding array in the calling sequence in the main program is available. Because of the statement

DIMENSION LR(58)

early in the subroutine, LL must not exceed 58. LINEQ(LL,C) uses the subprogram CABS. Also, since the matrix elements are complex, complex addition, subtraction, multiplication and division routines are tacitly assumed.

The second subroutine POT(AC,GS) computes $f(\phi_m)$ of (53). The variables in common are

$$RR1 = \rho_q \sin v_q - (z_p - z_q) \cos v_q$$

$$RR2 = -\rho_p \sin v_q$$

$$RR3 = \rho_q^2 + \rho_p^2 + (z_p - z_q)^2$$

$$RR4 = -2\rho_p\rho_q$$

$$BK = k$$

The arguments of POT are

$$AC = \cos \phi_m$$

$$GS = f(\phi_m)$$

GS is the only output of the subroutine POT(AC,GS). RR1, RR2 and AC are combined to give t_o of (50). RR3 and RR4 are used to find R_{pq}. When in (53) $\sqrt{t_1^2+d^2}$ is much larger than 1/4, the argument of the logarithm becomes close to one. Then, the series expansion for log(1+x) could possibly have been used in the subroutine POT(AC,GS), but was not. The subroutine POT(AC,GS) uses the subprograms ALOG, SIN, COS, CMPLX, ABS, and SQRT.

First of all, the main program reads the punched card data and then prints it to be certain that it was entered correctly. The constants π and η are inserted just after statement 47. The DO loop 2 puts ϕ_j appearing in (46) into ANG(J) and cos ϕ_j in AC(J). The DO loop 10 puts $\frac{\pi}{M}$ cos $(n-1)\phi_j$, j running from 1 to NPHI, in CSM(1) through CSM(NPHI), $\frac{\pi}{M}$ cos $n\phi_j$ in CSM(NPHI+1) through CSM(2*NPHI), and $\frac{\pi}{M}$ cos $(n+1)\phi_j$ in CSM(2*NPHI+1) through CSM(3*NPHI).

The nested DO loops 16 and 17 compute the G_n of (52). Actually, for the fixed n appearing in (45), G_{n-1}, G_n and G_{n+1} are needed. All are put in the linear complex array G. The G_{n-1} are put in G(1) through G(NG), G_n in G(NG+1) through G(2*NG), and G_{n+1} in G(2*NG+1) through G 3*NG). G_{n-1} is a KG by KG array. (KG=2*N and NG=KG*KG). The complex number G_{n-1}((J-1)*KG+I) is for the field point at I and the source in the vicinity of J. In DO loop 5, the subroutine POT is called upon to put $f(\phi_K)$ of (53) into GS(K). If (I=J), the logarithm expression of (58) instead of $f(\phi_1)$ is put into GS(1). The DO loop 13 performs the summation (52). The outer DO loop 68 obtains the cases (n-1), n,and (n+1).

After the G's are printed by statement 58, the numbers of (41) are inserted into the arrays T and TP. The impedance matrix (45) is computed in the nested DO loops 30 and 31. I and J correspond to the i and j of (42). The subscripts for Z^{tt}, $Z^{\phi t}$, $Z^{t\phi}$,and $Z^{\phi\phi}$ are respectively L1, L2, L3, L4 so that the impedance matrix with the submatrix arrangement of (25) is put columnwise into the linear complex array Z. The nested DO loops 70 and 71 perform the double sum in (45). II corresponds to p and JJ to q.

The logic between statements 84 and 89 is a routine to print Z. The statement

```
CALL LINEQ (NM2,Z)
```

inverts the impedance matrix. The admittance matrix now occupying Z is printed in DO loop 93. The data included at the end of Section A-3 is for a sphere with

```
NN = 1
 N = 10
NPHI = 20
BK = 0.3947842
```

BK is the propagation constant for a radius of 0.2 wavelengths. The portion of the data defining the geometry of the sphere was actually computed and punched on cards by a short auxiliary computer program.

If N or NPHI is too large, the dimension of some arrays must be increased. All the arrays whose dimension depends upon N or NPHI are listed below.

```
COMPLEX Z(NM2**2), GS(NPHI), G(12*N*N)
DIMENSION VS(N*2), SV(N*2), CV(N*2), ZS(N*2),
          R(N*2), ANG(NPHI), AC(NPHI),
          CSM(3*NPHI)
```

Here, as in the program,

```
NM2 = 2*(N-1).
```

A-3. The computer program

```
//REV170   JOB (0034,EE,11,03),'MAUTZ,JOE',MSGLEVEL=1
// EXEC FORTGCLG,PARM.FORT='MAP',PARM.LKED='XREF'
//FORT.SYSIN DD *
      SUBROUTINE LINEQ(LL,C)
      COMPLEX C(1),STOR,STO,ST,S
      DIMENSION LR(58)
      DO 20 I=1,LL
      LR(I)=I
   20 CONTINUE
      M1=0
      DO 18 M=1,LL
      K=M
      DO 2 I=M,LL
      K1=M1+I
      K2=M1+K
      IF(CABS(C(K1))-CABS(C(K2))) 2,2,6
    6 K=I
    2 CONTINUE
      LS=LR(M)
      LR(M)=LR(K)
      LR(K)=LS
      K2=M1+K
      STOR=C(K2)
      J1=0
      DO 7 J=1,LL
      K1=J1+K
      K2=J1+M
      STO=C(K1)
      C(K1)=C(K2)
      C(K2)=STO/STOR
      J1=J1+LL
    7 CONTINUE
      K1=M1+M
      C(K1)=1./STOR
      DO 11 I=1,LL
      IF(I-M) 12,11,12
   12 K1=M1+I
      ST=C(K1)
      C(K1)=0.
      J1=0
      DO 10 J=1,LL
      K1=J1+I
      K2=J1+M
      C(K1)=C(K1)-C(K2)*ST
      J1=J1+LL
   10 CONTINUE
   11 CONTINUE
      M1=M1+LL
   18 CONTINUE
      J1=0
      DO 9 J=1,LL
      IF(J-LR(J)) 14,8,14
   14 LRJ=LR(J)
      J2=(LRJ-1)*LL
   21 DO 13 I=1,LL
      K2=J2+I
      K1=J1+I
      S=C(K2)
      C(K2)=C(K1)
      C(K1)=S
```

```
13 CONTINUE
   LR(J)=LR(LRJ)
   LR(LRJ)=LRJ
   IF(J-LR(J)) 14,8,14
 8 J1=J1+LL
 9 CONTINUE
   RETURN
   END
   SUBROUTINE POT(AC,GS)
   COMMON RR1,RR2,RR3,RR4,BK
   COMPLEX W3,W4,GS,G
   YS=RR1+AC*RR2
   Y=ABS(YS)
   RD=RR3+RR4*AC
   RK=BK*SQRT(RD)
   D2=RD-Y*Y
   Y1=Y-.25
   Y2=Y+.25
   R1=SQRT(Y1*Y1+D2)
   R2=SQRT(Y2*Y2+D2)
   IF(Y1) 6,7,7
 6 TIN=2.*ALOG((-Y1+R1)*(Y2+R2)/D2)
   GO TO 8
 7 TIN =2.*ALOG((Y2+R2)/(Y1+R1))
 8 SN=SIN(RK)
   CS=COS(RK)
   S=BK-RK*TIN
   W3=CMPLX(CS,-SN)
   W4=CMPLX(TIN,-S)
   GS=W3*W4
   RETURN
   END
   COMMON RR1,RR2,RR3,RR4,BK
   COMPLEX A3,A4,Z(3364),GS(40),G(4800)
   DIMENSIONVS(60),SV(60),CV(60),ZS(60),R(60),ANG(40),AC(40),CSM(120)
   DIMENSION TP(4),T(4),JK(4)
 1 REWIND 4
50 READ(1,51,END=52)NN,N,NPHI,BK
51 FORMAT(3I3,E14.7)
   KG=2*N
61 READ(1,53)(VS(J),J=1,KG)
62 READ(1,53)(ZS(J),J=1,KG)
63 READ(1,53)(R(J),J=1,KG)
53 FORMAT(10F8.4)
   WRITE(3,54)NN,N,NPHI,BK
54 FORMAT(1X//' NN=',I3,' N=',I3,' NPHI=',I3,' BK=',E14.7)
55 FORMAT(1X/' VS')
56 FORMAT(1X/' ZS')
57 FORMAT(1X/' R')
   WRITE(3,55)
   WRITE(3,46)(VS(J),J=1,KG)
46 FORMAT(1X,10F8.4)
   WRITE(3,56)
   WRITE(3,46)(ZS(J),J=1,KG)
   WRITE(3,57)
   WRITE(3,46)(R(J),J=1,KG)
   DO 47 J=1,KG
   SV(J)=SIN(VS(J))
   CV(J)=COS(VS(J))
47 CONTINUE
```

```
      PI=3.141593
      ETA=376.707
      NM=N-1
      NM2=NM*2
      NZ=NM2*NM2
      NG=KG*KG
      M5=NN+2
      M6=NN+4
      FM=NN
      FM2=NN*NN
      DP=PI/NPHI
      DO 2 J=1,NPHI
      ANG(J)=(J-.5)*DP
      AC(J)=COS(ANG(J))
    2 CONTINUE
      M3=0
      DO 10 MM=M5,M6
      M1=MM-3
      M2=M3*NPHI
      DO 11 K=1,NPHI
      K1=M2+K
      CSM(K1)=DP*COS(M1*ANG(K))
   11 CONTINUE
      M3=M3+1
   10 CONTINUE
      CALL CLOCK(I1,I2)
      WRITE(3,99)I1,I2
   99 FORMAT(1X,2I7)
      DO 16 J=1,KG
      AA=DP*R(J)*.5
      DO 17 I=1,KG
      Z3=ZS(J)-ZS(I)
      RR1=SV(J)*R(J)+CV(J)*Z3
      RR2=-SV(J)*R(I)
      RR3=R(J)*R(J)+R(I)*R(I)+Z3*Z3
      RR4=-2.*R(J)*R(I)
   21 DO 5 K=2,NPHI
      CALL POT(AC(K),GS(K))
    5 CONTINUE
      IF(I-J) 7,8,7
    8 X=R(J)*DP
      XX=SQRT(1./16.+X*X)
      W1=(2.*X*ALOG((.25+XX)/X)+.5*ALOG((X+XX)/.25))/AA
      W2=-BK
      GS(1)=W1+(0.,1.)*W2
      GO TO 67
    7 CALL POT(AC(1),GS(1))
   67 M3=(J-1)*KG+I
      DO 68 MM=1,3
      M1=MM-1
      M4=M1*NPHI
      M2=M1*NG+M3
      G(M2)=0.
      DO 13 K=1,NPHI
      K2=K+M4
      G(M2)=G(M2)+GS(K)*CSM(K2)
   13 CONTINUE
   68 CONTINUE
   17 CONTINUE
   16 CONTINUE
```

```
      CALL CLOCK(I1,I2)
      WRITE(3,99)I1,I2
      WRITE(3,48)
   48 FORMAT(1X/' POTENTIALS FROM THE CIRCULAR RIBBONS OF CHARGE')
   58 WRITE(3,64)(G(K),K=1,NG)
   64 FORMAT(1X/(1X,10G11.4))
      CALL CLOCK(I1,I2)
      WRITE(3,99)I1,I2
      TP(1)=.5
      TP(2)=.5
      TP(3)=-.5
      TP(4)=-.5
      T(1)=.125
      T(2)=.375
      T(3)=.375
      T(4)=.125
      CA=BK*ETA
      CQ=CA/BK/BK
      DO 30 J=1,NM
      J1=2*(J-1)
      JL=(J-1)*NM2
      DO 31 I=1,NM
      L1=JL+I
      L2=L1+NM
      L3=L1+NM2*NM
      L4=L3+NM
      Z(L1)=0.
      Z(L2)=0.
      Z(L3)=0.
      Z(L4)=0.
      I1=2*(I-1)
      DO 70 JJ=1,4
      J2=J1+JJ
      KA1=(J2-1)*KG
      KB1=KA1+NG
      KC1=KB1+NG
      DO 71 II=1,4
      I2=I1+II
      SS=SV(I2)*SV(J2)
      CC=CV(I2)*CV(J2)
      KA2=KA1+I2
      KB2=KB1+I2
      KC2=KC1+I2
      A3=.5*(G(KC2)+G(KA2))
      A4=.5*(G(KC2)-G(KA2))
   74 Z(L1)=Z(L1)+(CA*T(II)*T(JJ)*(SS*A3+CC*G(KB2))-CQ*TP(II)*TP(JJ)*G(K
     1B2))*(0.,1.)
      Z(L2)=Z(L2)+CA*SV(J2)*T(II)*T(JJ)*A4-FM*CQ*G(KB2)*T(II)*TP(JJ)/R(I
     12)
      Z(L3)=Z(L3)-CA*SV(I2)*T(II)*T(JJ)*A4+FM*CQ*G(KB2)*TP(II)*T(JJ)/R(J
     12)
      Z(L4)=Z(L4)+(CA*A3-FM2*CQ/R(I2)/R(J2)*G(KB2))*T(II)*T(JJ)*(0.,1.)
   71 CONTINUE
   70 CONTINUE
   31 CONTINUE
   30 CONTINUE
      CALL CLOCK(I1,I2)
      WRITE(3,99)I1,I2
   84 JK(1)=1
      JK(2)=N
```

```
      JK(3)=NM2*NM+1
      JK(4)=JK(3)+NM
      DO 89 J=1,4
      K1=JK(J)
      WRITE(3,49)J
   49 FORMAT(1X/' Z',I1)
      DO 90 I=1,NM
      K2=K1+NM-1
   95 WRITE(3,88)(Z(K),K=K1,K2)
   88 FORMAT(1X,12G11.4)
      K1=K1+NM2
   90 CONTINUE
   89 CONTINUE
   33 WRITE (4)(Z(I),I=1,NZ)
      CALL CLOCK(I1,I2)
      WRITE(3,99) I1,I2
      CALL LINEQ(NM2,Z)
      CALL CLOCK(I1,I2)
      WRITE(3,99) I1,I2
      DO 93 J=1,4
      K1=JK(J)
      WRITE(3,24)J
   24 FORMAT(1X/' Y',I1)
      DO 92 I=1,NM
      K2=K1+NM-1
   96 WRITE(3,88)(Z(K),K=K1,K2)
      K1=K1+NM2
   92 CONTINUE
   93 CONTINUE
   34 WRITE (4)(Z(I),I=1,NZ)
      CALL CLOCK(I1,I2)
      WRITE(3,99)I1,I2
      GO TO 50
   52 STOP
      END
/*
//GO.FT04F001 DD DSNAME=EE0034.REV,DISP=OLD,UNIT=2314,                  X
//             VOLUME=SER=SU0004,DCB=(RECFM=V,BLKSIZE=1800,LRECL=1796)
//GO.SYSIN DD *
001010020 0.3947842E+00
  1.4923   1.3352   1.1781   1.0210   0.8639   0.7069   0.5498   0.3927   0.2356   0.0785
 -0.0785  -0.2356  -0.3927  -0.5498  -0.7069  -0.8639  -1.0210  -1.1781  -1.3352  -1.4923
  0.0098   0.0879   0.2423   0.4691   0.7627   1.1158   1.5199   1.9650   2.4400   2.9334
  3.4328   3.9262   4.4012   4.8463   5.2504   5.6035   5.8971   6.1239   6.2782   6.3564
  0.2497   0.7431   1.2181   1.6632   2.0673   2.4204   2.7140   2.9408   3.0951   3.1733
  3.1733   3.0951   2.9408   2.7140   2.4204   2.0673   1.6632   1.2181   0.7431   0.2497
/*
```

```
NN=  1 N= 10 NPHI= 20 GK= 0.3947842E 00

VS
  1.4923  1.3352  1.1781  1.0210  0.8639  0.7069  0.5498  0.3927  0.2356  0.0785
 -0.0785 -0.2356 -0.3927 -0.5498 -0.7069 -0.8639 -1.0210 -1.1781 -1.3352 -1.4923

ZS
  0.0098  0.0879  0.2423  0.4691  0.7627  1.1158  1.5199  1.9650  2.4400  2.9334
  3.4378  3.9262  4.4012  4.8463  5.2504  5.6035  5.8971  6.1239  6.2787  6.3564

R
  0.2497  0.7431  1.2181  1.6632  2.0673  2.4204  2.7140  2.9408  3.0951  3.1733
  3.1733  3.0951  2.9408  2.7140  2.4204  2.0673  1.6632  1.2181  0.7431  0.2497
  48630  68089
  48658  68089

POTENTIALS FROM THE CIRCULAR RIBBONS OF CHARGE

  12.76     -1.237      4.200     -1.221      2.266     -1.190      1.424     -1.145      0.9256    -1.089
 0.5880     -1.023     0.3421     -0.9506     0.1562    -0.8744    0.1351E-01-0.7969    -0.9662E-01-0.7204
-0.1812     -0.6470    -0.2454    -0.5784    -0.2935    -0.5158    -0.3289     -0.4602    -0.3544     -0.4121
-0.3722     -0.3719    -0.3843    -0.3398    -0.3921    -0.3157    -0.3967     -0.2997    -0.3988     -0.2917
  4.346     -1.222      5.392     -1.205      2.548     -1.176      1.509      -1.133     0.9670     -1.078
 0.6142     -1.015     0.3617     -0.9450     0.1724    -0.8712    0.2742E-01-0.7959    -0.8446E-01-0.7214
-0.1706     -0.6498    -0.2363    -0.5827    -0.2858    -0.5212    -0.3225     -0.4664    -0.3491     -0.4190
-0.3679     -0.3793    -0.3808    -0.3474    -0.3893    -0.3235    -0.3943     -0.3076    -0.3967     -0.2997
  2.295     -1.191      2.590     -1.176      3.456     -1.148      1.774      -1.108     1.068      -1.058
 0.6723     -0.9992    0.4031     -0.9340     0.2057    -0.8648    0.5575E-01-0.7939    -0.5984E-01-0.7234
-0.1491     -0.6553    -0.2178    -0.5910    -0.2701    -0.5318    -0.3093     -0.4789    -0.3383     -0.4327
-0.3591     -0.3939    -0.3737    -0.3627    -0.3834    -0.3392    -0.3893     -0.3236    -0.3921     -0.3157
  1.434     -1.146      1.522     -1.133      1.793     -1.109      2.507      -1.073     1.312      -1.029
 0.7809     -0.9751    0.4727     -0.9175     0.2587    -0.8552    0.9969E-01-0.7906    -0.2209E-01-0.7260
-0.1164     -0.6629    -0.1895    -0.6029    -0.2459    -0.5473    -0.2890     -0.4971    -0.3213     -0.4530
-0.3451     -0.4157    -0.3621    -0.3855    -0.3737    -0.3627    -0.3808     -0.3475    -0.3842     -0.3398
 0.9309     -1.089     0.9727     -1.079      1.075     -1.059      1.323      -1.029     1.943      -0.9910
 1.012      -0.9463    0.5876     -0.8963     0.3375    -0.8422    0.1619     -0.7858    0.3020E-01-0.7286
-0.7141E-01-0.6722    -0.1507    -0.6179    -0.2125    -0.5671    -0.2605     -0.5206    -0.2973     -0.4795
-0.3249     -0.4444    -0.3451    -0.4157    -0.3591    -0.3940    -0.3679     -0.3793    -0.3721     -0.3720
 0.5910     -1.024     0.6173     -1.016      0.6757    -0.9998    0.7850     -0.9765    1.019      -0.9466
 1.584      -0.9107    0.8127     -0.8702     0.4585    -0.8259    0.2486     -0.7791    0.9986E-01-0.7308
-0.1253E-01-0.6825    -0.1000    -0.6353    -0.1688    -0.5905    -0.2228     -0.5489    -0.2650     -0.5117
-0.2972     -0.4795    -0.3212    -0.4531    -0.3382    -0.4328    -0.3490     -0.4191    -0.3543     -0.4122
 0.3439     -0.9512    0.3636     -0.9456     0.4051    -0.9345    0.4749     -0.9181    0.5902     -0.8966
 0.8170     -0.8704    1.348      -0.8401     0.6817    -0.8065    0.3754     -0.7702    0.1932     -0.7321
 0.6350E-01-0.6932    -0.3540E-01-0.6543    -0.1130    -0.6167    -0.1744     -0.5813    -0.2228     -0.5490
-0.2604     -0.5207    -0.2889    -0.4972    -0.3093    -0.4790    -0.3224     -0.4666    -0.3288     -0.4603
 0.1574     -0.8749    0.1736     -0.8717     0.2069    -0.8653    0.2600     -0.8556    0.3390     -0.8425
 0.4602     -0.8262    0.6845     -0.8066     1.198     -0.7841    0.5999     -0.7590    0.3262     -0.7320
 0.1634     -0.7034    0.4683E-01-0.6741    -0.4251E-01-0.6449    -0.1129     -0.6167    -0.1687     -0.5905
-0.2124     -0.5672    -0.2458    -0.5474    -0.2700    -0.5320    -0.2857     -0.5214    -0.2934     -0.5160
 0.1428E-01-0.7973    0.2821E-01-0.7964    0.5655E-01-0.7944    0.1005     -0.7910    0.1628     -0.7861
 0.2495     -0.7793    0.3765     -0.7704    0.6016     -0.7591    1.108      -0.7457    0.5553     -0.7300
 0.3036     -0.7126    0.1540     -0.6938    0.4692E-01-0.6741    -0.3525E-01-0.6544    -0.9982E-01-0.6355
-0.1505     -0.6181    -0.1893    -0.6031    -0.2176    -0.5912    -0.2361     -0.5829    -0.2452     -0.5787
-0.9611E-01-0.7208    -0.8395E-01-0.7218    -0.5932E-01-0.7238    -0.2156E-01-0.7263    0.3073E-01-0.7289
 0.1004     -0.7310    0.1938     -0.7323    0.3268     -0.7321    0.5561     -0.7301    1.066      -0.7262
 0.5415     -0.7203    0.3038     -0.7127    0.1636     -0.7035    0.6381E-01-0.6933    -0.1221E-01-0.6827
-0.7108E-01-0.6724    -0.1160    -0.6631    -0.1488    -0.6555    -0.1702     -0.6502    -0.1808     -0.6473
-0.1808     -0.6473    -0.1702    -0.6501    -0.1488    -0.6555    -0.1160     -0.6631    -0.7107E-01-0.6724
-0.1221E-01-0.6827    0.6381E-01-0.6933    0.1636     -0.7035    0.3038     -0.7126    0.5415     -0.7203
  1.066     -0.7262    0.5561     -0.7301    0.3268     -0.7321    0.1938     -0.7323    0.1004     -0.7310
 0.3073E-01-0.7289    -0.2156E-01-0.7263    -0.5932E-01-0.7238    -0.8393E-01-0.7218    -0.9611E-01-0.7208
-0.2457     -0.5787    -0.2361     -0.5829    -0.2176     -0.5912    -0.1893     -0.6031    -0.1505     -0.6181
-0.9982E-01-0.6355    -0.3525E-01-0.6544    0.4692E-01-0.6741    0.1540     -0.6938    0.3036     -0.7126
 0.5553     -0.7300    1.108      -0.7457    0.6016     -0.7591    0.3765     -0.7704    0.2495     -0.7793
 0.1628     -0.7661    0.1005     -0.7910    0.5655E-01-0.7944    0.2823E-01-0.7964    0.1428E-01-0.7973
-0.2934     -0.5160    -0.2857     -0.5214    -0.2700     -0.5320    -0.2458     -0.5474    -0.2124     -0.5672
-0.1687     -0.5905    -0.1129     -0.6167    -0.4251E-01-0.6449    0.4683E-01-0.6741    0.1634     -0.7034
 0.3262     -0.7320    0.5999     -0.7590     1.198      -0.7841    0.6845     -0.8066    0.4602     -0.8262
 0.3390     -0.8425    0.2600     -0.8556     0.2069     -0.8653    0.1736     -0.8717    0.1574     -0.8749
-0.3288     -0.4603    -0.3224     -0.4666    -0.3093     -0.4790    -0.2889     -0.4972    -0.2604     -0.5207
-0.2228     -0.5490    -0.1744     -0.5813    -0.1130     -0.6167    -0.3540E-01-0.6543    0.6350E-01-0.6932
 0.1932     -0.7321    0.3754     -0.7702     0.6817     -0.8065    1.348      -0.8401    0.8170     -0.8704
```

0.5902	-0.8966	0.4749	-0.9181	0.4051	-0.9345	0.3636	-0.9457	0.3439	-0.9512
-0.3543	-0.4122	-0.3490	-0.4191	-0.3382	-0.4328	-0.3212	-0.4531	-0.2972	-0.4795
-0.2650	-0.5117	-0.2228	-0.5489	-0.1688	-0.5905	-0.1000	-0.6353	-0.1253E-01	-0.6825
0.9986E-01	-0.7308	0.2486	-0.7791	0.4585	-0.8259	0.8127	-0.8702	1.584	-0.9107
1.019	-0.9466	0.7850	-0.9765	0.6757	-0.9998	0.6173	-1.016	0.5910	-1.024
-0.3721	-0.3720	-0.3679	-0.3793	-0.3591	-0.3940	-0.3451	-0.4157	-0.3249	-0.4444
-0.2973	-0.4795	-0.2605	-0.5206	-0.2125	-0.5671	-0.1507	-0.6179	-0.7141E-01	-0.6722
0.3019E-01	-0.7286	0.1619	-0.7858	0.3375	-0.8422	0.5876	-0.8963	1.012	-0.9463
1.943	-0.9910	1.323	-1.023	1.075	-1.059	0.9727	-1.079	0.9309	-1.089
-0.3842	-0.3398	-0.3808	-0.3474	-0.3737	-0.3627	-0.3621	-0.3855	-0.3491	-0.4157
-0.3213	-0.4530	-0.2890	-0.4971	-0.2459	-0.5473	-0.1895	-0.6029	-0.1164	-0.6629
-0.2209E-01	-0.7260	0.9969E-01	-0.7905	0.2587	-0.8552	0.4727	-0.9176	0.7809	-0.9761
1.312	-1.029	2.507	-1.073	1.793	-1.109	1.522	-1.133	1.434	-1.146
-0.3921	-0.3157	-0.3893	-0.3235	-0.3834	-0.3392	-0.3737	-0.3627	-0.3591	-0.3939
-0.3383	-0.4327	-0.3093	-0.4789	-0.2701	-0.5318	-0.2173	-0.5910	-0.1491	-0.6553
-0.5984E-01	-0.7234	0.5575E-01	-0.7939	0.2057	-0.8648	0.4031	-0.9340	0.6723	-0.9992
1.068	-1.058	1.774	-1.103	3.456	-1.148	2.590	-1.176	2.295	-1.191
-0.3967	-0.2997	-0.3943	-0.3076	-0.3893	-0.3235	-0.3808	-0.3474	-0.3679	-0.3793
-0.3491	-0.4190	-0.3225	-0.4665	-0.2858	-0.5212	-0.2363	-0.5827	-0.1705	-0.6498
-0.8444E-01	-0.7215	0.2744E-01	-0.7953	0.1724	-0.8712	0.3617	-0.9450	0.6142	-1.015
0.9671	-1.078	1.509	-1.133	2.549	-1.176	5.392	-1.205	4.346	-1.222
-0.3988	-0.2917	-0.3967	-0.2997	-0.3921	-0.3157	-0.3843	-0.3398	-0.3722	-0.3719
-0.3544	-0.4121	-0.3239	-0.4602	-0.2935	-0.5158	-0.2454	-0.5784	-0.1812	-0.6470
-0.9662E-01	-0.7204	0.1351E-01	-0.7969	0.1562	-0.8744	0.3421	-0.9506	0.5880	-1.023
0.9256	-1.089	1.424	-1.145	2.266	-1.190	4.200	-1.221	12.76	-1.237
48660	68089								
48668	68089								

Z1

53.46	-2477.	44.61	720.4	32.93	260.0	20.78	95.16	10.24	52.17	2.490	37.39
-2.342	32.88	-4.857	32.25	-5.909	32.68						
44.45	707.3	39.96	-1334.	32.26	413.2	23.45	182.9	14.73	76.37	7.101	47.40
1.234	36.85	-2.688	33.21	-4.859	32.25						
32.95	262.9	32.15	408.1	30.37	-962.5	26.13	324.3	20.30	158.8	13.48	72.10
6.766	46.93	1.236	36.86	-2.337	32.89						
20.81	95.56	23.44	183.9	26.13	322.2	27.15	-811.6	24.92	294.6	19.96	153.1
13.49	72.14	7.108	47.44	2.502	37.42						
10.26	52.28	14.74	76.52	20.29	159.2	24.90	293.9	26.80	-768.9	24.90	293.9
20.29	159.2	14.74	76.52	10.26	52.28						
2.501	37.42	7.109	47.44	13.48	72.14	19.96	153.1	24.92	294.6	27.15	-811.6
26.13	322.2	23.44	183.9	20.81	95.56						
-2.336	32.89	1.235	36.86	6.766	46.93	13.48	72.10	20.30	158.8	26.19	324.3
30.37	-962.5	32.15	408.1	32.93	262.9						
-4.858	32.25	-2.688	33.21	1.234	36.85	7.100	47.40	14.73	76.37	23.45	182.9
32.26	413.2	39.96	-1334.	44.45	707.3						
-5.909	32.68	-4.859	32.24	-2.342	32.87	2.491	37.39	10.24	52.17	20.78	95.16
32.93	260.0	44.61	720.4	53.46	-2477.						

Z2

-1551.	54.68	371.7	50.24	86.50	43.28	44.68	35.22	37.17	27.15	35.32	19.89
34.48	14.31	33.79	9.762	33.29	7.222						
-769.1	45.11	-180.7	41.49	174.2	36.17	63.52	29.77	41.64	23.24	36.24	17.27
34.17	12.35	33.05	8.734	32.41	6.547						
-195.7	32.13	-291.0	29.63	-55.36	26.00	128.3	21.65	57.89	17.02	40.84	12.67
35.54	8.937	33.22	6.221	32.13	4.517						
-81.33	18.80	-100.8	17.26	-168.9	14.91	-17.79	12.07	116.8	9.018	58.76	6.009
42.75	3.371	37.26	1.340	34.95	0.6566E-01						
-46.57	7.677	-52.14	6.529	-59.02	4.732	-126.4	2.466	0.2136E-03	-0.1984E-03	126.4	-2.466
69.02	-4.732	52.14	-6.529	46.57	-7.677						
-34.96	-0.6591E-01	-37.26	-1.341	-42.75	-3.371	-58.76	-6.009	-116.8	-9.019	17.79	-12.07
168.9	-14.91	100.8	-17.26	91.33	-14.80						
-32.13	-4.517	-33.22	-6.222	-35.54	-8.988	-40.84	-12.67	-57.89	-17.02	-128.3	-21.65
55.37	-26.00	291.0	-29.63	195.7	-32.13						
-32.41	-8.547	-33.05	-8.734	-34.17	-12.35	-36.24	-17.27	-41.64	-23.24	-63.52	-29.77
-174.2	-36.17	180.7	-41.49	764.1	-45.11						
-33.28	-7.222	-33.79	-9.763	-34.48	-14.01	-35.32	-19.90	-37.17	-27.15	-44.68	-35.22
-86.50	-43.28	-371.7	-50.24	1551.	-54.68						

Z3

1569.	-54.38	758.4	-45.05	193.8	-32.05	80.96	-18.75	46.46	-7.653	34.93	0.7282E-01
32.12	4.519	32.41	6.547	33.28	7.222						
-370.3	-50.31	184.8	-41.58	289.6	-29.62	100.3	-17.23	52.02	-6.510	37.23	1.348
33.21	6.224	33.05	8.736	33.79	9.767						
-86.91	-43.31	-173.9	-36.22	56.65	-26.04	167.6	-14.91	68.86	-4.719	42.71	3.380
35.53	8.993	34.16	12.35	34.47	14.02						
-44.68	-35.26	-63.63	-29.80	-128.2	-21.68	18.23	-12.09	126.3	-2.462	58.71	6.018
40.83	12.68	34.23	17.28	35.31	19.91						
-37.15	-27.17	-41.63	-23.26	-57.91	-17.04	-116.7	-9.032	-0.1678E-03	0.3433E-04	116.7	9.032
57.91	17.04	41.63	23.26	37.15	27.17						
-35.31	-19.91	-36.23	-17.28	-40.83	-12.68	-58.71	-6.017	-126.3	2.462	-18.23	12.09
128.2	21.68	63.63	29.80	44.68	35.26						
-34.48	-14.02	-34.16	-12.35	-35.53	-8.993	-42.71	-3.380	-68.86	4.720	-167.6	14.91
-56.65	26.04	173.9	36.22	86.91	43.31						
-33.79	-9.766	-33.05	-8.736	-33.21	-6.225	-37.23	-1.348	-52.02	6.510	-100.3	17.23
-289.6	29.62	-184.8	41.58	370.3	50.31						
-33.28	-7.223	-32.41	-6.547	-32.12	-4.519	-34.93	-0.7334E-01	-46.46	7.653	-80.96	18.75
-193.8	32.05	-758.4	45.05	-1569.	54.88						

Z4

57.67	-2641.	52.71	-264.4	45.69	-61.31	37.53	-37.68	29.26	-34.35	21.76	-34.27
15.61	-34.35	11.13	-34.18	8.426	-33.94						
52.66	-267.8	49.14	-176.2	43.74	-54.78	37.19	-30.95	30.27	-29.88	23.68	-31.54
18.04	-32.99	13.77	-33.82	11.13	-34.19						
45.68	-61.62	43.73	-54.99	40.56	-28.89	36.37	-16.08	31.51	-21.69	26.47	-26.76
21.80	-30.51	18.04	-32.99	15.61	-34.36						
37.53	-37.73	37.19	-30.98	36.37	-16.07	34.83	2.746	32.51	-5.667	29.59	-19.25
26.47	-26.76	23.68	-31.54	21.76	-34.27						
29.26	-34.36	30.27	-29.88	31.51	-21.68	32.51	-5.656	32.90	9.467	32.51	-5.656
31.51	-21.68	30.27	-29.88	29.26	-34.37						
21.76	-34.27	23.68	-31.54	26.47	-26.76	29.59	-19.25	32.51	-5.667	34.83	2.746
36.37	-16.07	37.19	-30.98	37.53	-37.73						
15.61	-34.36	18.04	-32.99	21.80	-30.51	26.47	-26.76	31.51	-21.69	36.37	-16.08
40.56	-28.89	43.73	-54.99	45.68	-61.62						
11.13	-34.18	13.77	-33.82	18.04	-32.99	23.68	-31.54	30.27	-29.88	37.19	-30.95
43.74	-54.78	49.14	-176.2	52.66	-267.8						
8.425	-33.94	11.13	-34.18	15.61	-34.35	21.76	-34.27	29.26	-34.35	37.53	-37.68
45.69	-61.31	52.71	-264.4	57.67	-2641.						
48669	68089										
48671	68089										

Y1

0.3630E-04-0.1602E-02 0.5820E-04-0.4313E-03 0.5949E-04 0.1440E-03 0.4360E-04-0.3064E-03 0.1936E-04 0.2109E-04-0.2334E-05-0.1297E-03
-0.1513E-04 0.2209E-05-0.1719E-04-0.7371E-04-0.1087E-04 0.8885E-04
0.5760E-04-0.4297E-03 0.9620E-04-0.4419E-03 0.1053E-03-0.3705E-03 0.8639E-04-0.5315E-04 0.5012E-04-0.2126E-03 0.1222E-04-0.7892E-04
-0.1442E-04-0.1056E-03-0.2375E-04-0.1337E-04-0.1693E-04-0.7437E-04
0.5875E-04 0.1515E-03 0.1049E-03-0.3712E-03 0.1269E-03-0.4147E-04 0.1196E-03-0.2268E-03 0.8816E-04-0.8841E-04 0.4484E-04-0.1642E-03
0.6789E-05-0.9457E-04-0.1436E-04-0.1055E-03-0.1482E-04 0.3451E-05
0.4313E-04-0.3103E-03 0.8620E-04-0.5167E-04 0.1196E-03-0.2281E-03 0.1328E-03 0.2438E-03 0.1205E-03-0.1497E-03 0.8590E-04-0.7541E-04
0.4478E-04-0.1645E-03 0.1220E-04-0.7833E-04-0.2206E-05-0.1305E-03
0.1921E-04 0.2524E-04 0.4995E-04-0.2131E-03 0.8805E-04-0.8821E-04 0.1204E-03-0.1499E-03 0.1342E-03 0.3588E-03 0.1204E-03-0.1499E-03
0.8805E-04-0.8821E-04 0.4995E-04-0.2131E-03 0.1921E-04 0.2524E-04
-0.2201E-05-0.1305E-03 0.1220E-04-0.7833E-04 0.4478E-04-0.1645E-03 0.8590E-04-0.7541E-04 0.1205E-03-0.1497E-03 0.1328E-03 0.2438E-03
0.1196E-03-0.2281E-03 0.8620E-04-0.5167E-04 0.4312E-04-0.3104E-03
-0.1482E-04 0.3456E-05-0.1436E-04-0.1055E-03 0.6789E-05-0.9457E-04 0.4484E-04-0.1642E-03 0.8816E-04-0.8841E-04 0.1196E-03-0.2268E-03
0.1269E-03-0.4147E-04 0.1049E-03-0.3712E-03 0.5875E-04 0.1515E-03
-0.1693E-04-0.7436E-04-0.2375E-04-0.1337E-04-0.1442E-04-0.1056E-03 0.1222E-04-0.7892E-04 0.5012E-04-0.2126E-03 0.8638E-04-0.5315E-04
0.1053E-03-0.3705E-03 0.9620E-04-0.4419E-03 0.5759E-04-0.4298E-03
-0.1085E-04 0.9884E-04-0.1719E-04-0.7370E-04-0.1513E-04 0.2210E-05-0.2334E-05-0.1297E-03 0.1936E-04 0.2109E-04 0.4360E-04-0.3064E-03
0.5949E-04 0.1440E-03 0.5820E-04-0.4313E-03 0.3630E-04-0.1602E-02

Y2

0.1646E-02 0.3722E-04-0.6393E-02 0.5860E-04 0.4903E-02 0.6929E-04-0.3836E-02 0.6055E-04 0.2336E-02 0.5216E-04-0.1599E-02 0.3940E-04
0.9628E-03 0.3111E-04-0.5332E-03 0.2106E-04 0.7572E-04 0.1125E-04
0.4137E-03 0.5873E-04 0.9168E-03 0.9430E-04-0.3702E-02 0.1111E-03 0.1864E-02 0.9790E-04-0.1605E-02 0.8236E-04 0.8067E-03 0.6145E-04
-0.6478E-03 0.4852E-04 0.2596E-03 0.3165E-04-0.6571E-04 0.1780E-04
-0.1004E-03 0.5930E-04 0.1907E-02 0.9996E-04-0.4048E-03 0.1126E-03-0.2265E-02 0.1023E-03 0.7880E-03 0.8157E-04-0.9142E-03 0.5743E-04
0.3259E-03 0.4454E-04-0.3249E-03 0.2555E-04-0.3046E-05 0.1616E-04
0.2872E-03 0.4274E-04-0.8422E-03 0.7768E-04 0.2504E-02 0.8042E-04-0.4017E-03 0.7278E-04-0.2151E-02 0.5086E-04 0.7298E-03 0.2596E-04
-0.8830E-03 0.1618E-04 0.2162E-03 0.4530E-06-0.1229E-03 0.3737E-05
-0.4706E-05 0.1798E-04 0.8233E-03 0.3817E-04-0.8928E-03 0.3086E-04 0.2374E-02 0.2304E-04-0.9505E-08 0.8877E-09-0.2374E-02-0.2304E-04
0.8927E-03-0.3086E-04-0.8233E-03-0.3817E-04 0.4705E-05-0.1798E-04
0.1229E-03-0.3733E-05-0.2162E-03-0.4676E-06 0.8830E-03-0.1615E-04-0.7298E-03-0.2598E-04 0.2151E-02-0.5085E-04 0.4018E-03-0.7279E-04
-0.2504E-02-0.8042E-04 0.8422E-03-0.7769E-04-0.2872E-03-0.4273E-04
0.3043E-05-0.1617E-04 0.3250E-03-0.2555E-04-0.3260E-03-0.4455E-04 0.9142E-03-0.5742E-04-0.7881E-03-0.8158F-04 0.2265E-02-0.1023E-03
0.4048E-03-0.1126E-03-0.1907E-02-0.9996E-04 0.1004E-03-0.5930E-04
0.6570E-04-0.1780E-04-0.2596E-03-0.3163E-04 0.6478E-03-0.4854E-04-0.8067E-03-0.6141E-04 0.1605E-02-0.8237E-04-0.1864E-02-0.9790E-04
0.3702E-02-0.1111E-03-0.9168E-03-0.9431E-04-0.4137E-03-0.5872E-04
-0.7573E-04-0.1123E-04 0.5332E-03-0.2111E-04-0.9627E-03-0.3103E-04 0.1599E-02-0.3941E-04-0.2336E-02-0.5215E-04 0.3836E-02-0.6054E-04
-0.4903E-02-0.6930E-04 0.6393E-02-0.5860E-04-0.1646E-02-0.3721E-04

Y3

-0.1650E-02-0.3725E-04-0.4173E-03-0.5935E-04 0.9465E-04-0.6004E-04-0.2850E-03-0.4315E-04 0.1328E-05-0.1805E-04-0.1226E-03 0.3953E-05
-0.3970E-05 0.1653E-04-0.6534E-04 0.1808E-04 0.7614E-04 0.1125E-04
0.6438E-02-0.5656E-04-0.9059E-03-0.9188E-04-0.1889E-02-0.9791E-04 0.8290E-03-0.7604E-04-0.8099E-03-0.3780E-04 0.2137E-03 0.1240E-06
-0.3215E-03 0.2466E-04 0.2591E-03 0.3061E-04-0.5382E-03 0.2013E-04
-0.5002E-02-0.6885E-04 0.3707E-02-0.1126E-03 0.4010E-03-0.1144E-03-0.2495E-02-0.8142E-04 0.8819E-03-0.3094E-04-0.8808E-03 0.1669E-04
0.3257E-03 0.4551E-04-0.6504E-03 0.4935E-04 0.9823E-03 0.3110E-04
0.3923E-02-0.5937E-04-0.1884E-02-0.9582E-04 0.2271E-02-0.1008E-03 0.4020E-03-0.7196E-04-0.2368E-02-0.2293E-04 0.7305E-03 0.2544E-04
-0.9174E-03 0.5652E-04 0.8158E-03 0.6021E-04-0.1636E-02 0.3841E-04
-0.2400E-02-0.5180E-04 0.1620E-02-0.8341E-04-0.7961E-03-0.8261E-04 0.2151E-02-0.5142E-04 0.7916E-08-0.9357E-08-0.2151E-02 0.5142E-04
0.7961E-03 0.8259E-04-0.1620E-02 0.8339E-04 0.2400E-02 0.5183E-04
0.1636E-02-0.3847E-04-0.8158E-03-0.6019E-04 0.9174E-03-0.5651E-04-0.7305E-03-0.2545E-04 0.2368E-02 0.2296E-04-0.4020E-03 0.7194E-04
-0.2271E-02 0.1009E-03 0.1884E-02 0.9585E-04-0.3923E-02 0.5935E-04
-0.9822E-03-0.3103E-04 0.6504E-03-0.4937E-04-0.3257E-03-0.4552E-04 0.8808E-03-0.1668F-04-0.8819E-03 0.3091E-04 0.2495E-02 0.8143E-04
-0.4010E-03 0.1144E-03-0.3707E-02 0.1125E-03 0.5002E-02 0.6886E-04
0.5381E-03-0.2020E-04-0.2591E-03-0.3061E-04 0.3215E-03-0.2465E-04-0.2137E-03-0.1294E-06 0.8098E-03 0.3781E-04-0.8290E-03 0.7604E-04
0.1889E-02 0.9792E-04 0.9059E-03 0.9190E-04-0.6438E-02 0.5656E-04
-0.7613E-04-0.1124E-04 0.6534E-04-0.1808E-04 0.3968E-05-0.1653E-04-0.1226E-03-0.3952E-05-0.1376E-05 0.1805E-04 0.2851E-03 0.4315E-04
-0.9466E-04 0.6004E-04 0.4173E-03 0.5935E-04 0.1650E-02 0.3725E-04

Y4

0.3829E-04-0.1231E-02 0.6015E-04 0.5634E-02 0.7181E-04-0.4170E-02 0.6314E-04 0.3319E-02 0.5466E-04-0.1995E-02 0.4150E-04 0.1380E-02
0.3251E-04-0.8249E-03 0.2206E-04 0.4599E-03 0.1163E-04-0.6498E-04
0.5795E-04 0.5654E-02 0.9621E-04-0.2768E-01 0.1289E-03 0.2989E-01 0.1240E-03-0.1999E-01 0.1110E-03 0.1358E-01 0.8669E-04-0.8456E-02
0.6454E-04 0.5520E-02 0.4115E-04-0.2812E-02 0.2106E-04 0.4617E-03
0.7150E-04-0.4235E-02 0.1354E-03 0.3013E-01 0.1711E-03-0.4857E-01 0.1966E-03 0.4095E-01 0.1819E-03-0.2524E-01 0.1489E-03 0.1680E-01
0.1079E-03-0.1039E-01 0.6729E-04 0.5570E-02 0.3251E-04-0.8375E-03
0.6175E-04 0.3378E-02 0.1220E-03-0.2026E-01 0.1953E-03 0.4112E-01 0.2190E-03-0.5381E-01 0.2363E-03 0.4246E-01 0.1959E-03-0.2564E-01
0.1468E-03 0.1638E-01 0.8640E-04-0.8573E-02 0.4037E-04 0.1405E-02
0.5434E-04-0.2040E-02 0.1156E-03 0.1379E-01 0.1801E-03-0.2540E-01 0.2397E-03 0.4252E-01 0.2509E-03-0.5426E-01 0.2397E-03 0.4252E-01
0.1804E-03-0.2540E-01 0.1155E-03 0.1379E-01 0.5437E-04-0.2040E-02
0.4043E-04 0.1405E-02 0.8620E-04-0.8572E-02 0.1471E-03 0.1688E-01 0.1957E-03-0.2564E-01 0.2363E-03 0.4246E-01 0.2191E-03-0.5381E-01
0.1959E-03 0.4112E-01 0.1222E-03-0.2026E-01 0.6172E-04 0.3378E-02
0.3244E-04-0.8375E-03 0.6752E-04 0.5570E-02 0.1075E-03-0.1039E-01 0.1491E-03 0.1680E-01 0.1819E-03-0.2524E-01 0.1965E-03 0.4095E-01
0.1713E-03-0.4857E-01 0.1353E-03 0.3013E-01 0.7151E-04-0.4235E-02
0.2114E-04 0.4617E-03 0.4093E-04-0.2812E-02 0.6488E-04 0.5520E-02 0.8659E-04-0.8456E-02 0.1110E-03 0.1358E-01 0.1240E-03-0.1999E-01
0.1288E-03 0.2989E-01 0.9624E-04-0.2768E-01 0.5794E-04 0.5654E-02
0.1162E-04-0.6499E-04 0.2209E-04 0.4595E-03 0.3246E-04-0.8248E-03 0.4149E-04 0.1380E-02 0.5467E-04-0.1995E-02 0.6312E-04 0.3319E-02
0.7183E-04-0.4170E-02 0.6014E-04 0.5636E-02 0.3829E-04-0.1231E-02
48673 6E089

REFERENCES

[1] R. F. Harrington, "Matrix Methods for Field Problems," Proc. IEEE, vol. 55, no. 2, Feb. 1967, pp. 136-149.

[2] R. F. Harrington, Field Computation by Moment Methods, The Macmillan Co., New York, 1968.

[3] R. F. Harrington, "Generalized Network Parameters in Field Theory," Proc. Sym. on Generalized Networks, MRIS Series, vol. XVI, Polytechnic Press, Brooklyn, N. Y., 1966, pp. 51-67.

[4] R. F. Harrington, "Theory of Loaded Scatterers," Proc. IEE (London), vol. 111, no. 4, April 1964, pp. 617-623.

[5] R. F. Harrington and J. R. Mautz, "Straight Wires with Arbitrary Excitation and Loading," IEEE Trans., vol. AP-15, no. 4, July 1967, pp. 502-515.

[6] M. G. Andreasen, "Scattering From Bodies of Revolution," IEEE Trans., vol. AP-13, no. 2, March 1965, pp. 303-310.

[7] H. B. Dwight, Tables of Integrals and Other Mathematical Data, The Macmillan Company, 1961, p. 50, Eq. 200.01.

[8] R. F. Harrington, Field Computation by Moment Methods, The Macmillan Co., New York, 1968, p. 70, Eq. 4-36.

[9] Ibid., p. 70, Eq. 4-37.

[10] Ibid., p. 90, Eq. 5-39.

[11] Ibid., Chapter 6.

[12] Ibid., Section 8-8.

[13] J. R. Mautz, Radiation and Scattering from Bodies of Revolution, Ph.D. thesis, Syracuse University, Syracuse, N. Y., May 1968, Appendix B.